Geochemistry Geophysics Geosystems G3

Article
Volume 12, Number 2
18 February 2011
Q02005, doi:10.1029/2010GC003398
ISSN: 1525-2027

Published by AGU and the Geochemical Society

Lateral constrictional flow of hot orogenic crust: Insights from the Neoarchean of south India, geological and geophysical implications for orogenic plateaux

Dominique Chardon
Université de Toulouse, UPS (OMP), GET, 14 Avenue Edouard Belin, F-31400 Toulouse, France (dominique.chardon@get.obs-mip.fr)

CNRS, GET, F-31400 Toulouse, France

IRD, GET, F-31400 Toulouse, France

Mudlappa Jayananda
Department of Geology, Centre of Advanced Studies, University of Delhi, Delhi 110 007, India

Jean-Jacques Peucat
Géosciences-Rennes, UMR CNRS 6118, Université de Rennes 1, F-35042 Rennes Cedex, France

[1] This study provides an in situ geological perspective on fabrics produced by synconvergence lateral crustal flow of hot orogens. It is based on the example of the Neoarchean orogen of the Dharwar craton (India) and combines structural analysis and ion microprobe U-Pb zircon geochronology. We document a pervasive, three-dimensional flow mode of the lower crust, called lateral constrictional flow (LCF), which combines orogen-normal shortening, lateral constrictional stretching, and transtension. LCF achieves gravity-driven flow, lateral escape, and 3-D mass redistribution in a viscous lower crust submitted to convergence. LCF tends to mechanically and thermally homogenize the lower crust and efficiently compensates topographic relief at a shallow level in the crust. Three type-geodynamic contexts are envisaged for LCF: plateau interiors, inner parts of collisional crustal wedges or plateau edges, and throughout wide ultrahot orogens such as the Neaoarchean orogen of south India. LCF makes the lower crust act as a strain gauge between lateral gravitational collapse or tectonic thickening of the upper crust, thrust stacking in the lowermost crust (collisional crustal wedge case), crustal shortening, and/or lateral flow of the upper mantle. In the case of plateau interiors or ultrahot orogens, LCF of a thick lower crust enables coupling of upper crustal deformation with upper mantle flow through a hot and thin lithosphere being shortened coherently. LCF generates a subhorizontal lamination that should produce the strong seismic reflectivity and lateral anisotropy of the Tibetan Plateau and a variety of hot orogens.

Components: 11,400 words, 13 figures, 1 table.

Keywords: crustal flow; hot orogen; seismic reflectivity; Tibet; Dharwar craton; Archean.

Index Terms: 8110 Tectonophysics: Continental tectonics: general (0905); 8102 Tectonophysics: Continental contractional orogenic belts and inversion tectonics; 8103 Tectonophysics: Continental cratons.

Received 19 October 2010; **Revised** 20 December 2010; **Accepted** 29 December 2010; **Published** 18 February 2011.

Chardon, D., M. Jayananda, and J.-J. Peucat (2011), Lateral constrictional flow of hot orogenic crust: Insights from the Neoarchean of south India, geological and geophysical implications for orogenic plateaux, *Geochem. Geophys. Geosyst.*, *12*, Q02005, doi:10.1029/2010GC003398.

1. Introduction

[2] In orogenic belts, crustal flow may be greatly facilitated by heating due to crustal thickening [*England and Thompson*, 1984], magmatic advection of mantle heat into the crust [*Wells*, 1980], or heat conduction through a thinned lithospheric mantle [*Sandiford and Powell*, 1991], resulting in partial melting and mechanical weakening of the orogens [*Vanderhaeghe and Teyssier*, 2001]. The hot orogen concept applies to orogens that have undergone pervasive partial melting in regions of attenuated mantle lithosphere, such as orogenic plateaux, mature collision zones, Cordilleras or back-arc domains, Precambrian accretionary orogens or magmatic arcs [*Chardon et al.*, 2009]. Hot orogens are therefore particularly prompt to flow under a precarious balance between shortening-induced thickening, gravity-driven thinning, and lateral and transversal flow [*Vanderhaeghe and Teyssier*, 2001; *Beaumont et al.*, 2004; *Schulmann et al.*, 2008; *Chardon et al.*, 2009]. In this paper, we are concerned with lateral flow as an end-member synconvergence flow mode of hot orogenic crust.

[3] Eastward lateral flow in Tibet is inferred to occur by channel-flow extrusion of lower crust driven by the gravitational potential energy gradient existing between the plateau and its eastern foreland [*Bird*, 1991; *Royden et al.*, 2008, and references therein]. The velocity field of lateral channel flow is that of two-dimensional heterogeneous simple shear in a vertical, orogen-parallel plane. But lateral flow of central Tibet interferes with transverse shortening and orogen-oblique stretching revealed by Late Cenozoic and active deformation patterns [*Andronicos et al.*, 2007]. Lateral flow is therefore fundamentally a three-dimensional process responding to the interplay of gravitational flow and tectonic shortening of hot orogens. Accordingly, the typically thick (ca. 15 s TWT), highly reflective and laterally anisotropic lower crust of Tibet [*Klemperer*, 2006] and most hot orogens [e.g., *Van Der Velden et al.*, 2006] cannot be a simple product of two-dimensional ductile extension or channel flow, as generally implied [e.g., *Meissner et al.*, 2006]. These seismic properties must indeed reflect fabrics produced by three-dimensional flow of the orogenic crust.

[4] As orogenic plateaux and Precambrian hot orogens have in common a very thin mantle lithosphere, orogenic flow somewhat comparable to that governing Precambrian hot orogens should operate through today's orogenic plateaux [*Cagnard et al.*, 2006a; *Chardon et al.*, 2009]. Furthermore, Precambrian hot orogens expose very large areas of crust preserved from post orogenic collapse [*Cagnard et al.*, 2006b; *Chardon et al.*, 2009]. Thus, studies of the lower crust exposed in Precambrian hot orogens may allow inferring the nature and origin of flow fabrics that are imaged by geophysical techniques beneath orogenic plateaux and active hot orogens.

[5] In this study, we combine structural analysis and ion microprobe U-Pb dating to investigate the development of the crustal fabric formed by synconvergence lateral flow of the Neoarchean orogen exposed by the wide crustal transition of the Dharwar craton. The study allows defining the three-dimensional kinematic framework of a bulk orogenic flow mode called lateral constrictional flow (LCF). We then evaluate the applicability of LCF to hot orogens in general and to the Himalayan-Tibet orogen in particular, with an emphasis on the relationships between LCF and upper mantle flow, upper crustal deformation and sedimentation, and thrust thickening. Finally, we show that the fabric formed by LCF may produce the strong seismic reflectivity and anisotropy of hot orogens.

2. Regional Framework

[6] The Dharwar craton consists of 3.4–2.7 Ga tonalite-trondhjemite-granodiorite (TTG) gneisses and greenstone belts emplaced between 3.3 and 2.6 Ga [e.g., *Peucat et al.*, 1993, 1995; *Chadwick et al.*, 2000, 2007; *Jayananda et al.*, 2000, 2006, 2008]. The craton was ultimately shaped between 2.56 and 2.50 Ga by a HT-LP tectonometamorphic episode that led to the development of a regional array of transcurrent shear zones [*Drury and Holt*, 1980; *Chardon et al.*, 2008]. The eastern branch of the Chitradurga shear zone system marks the boundary between the Eastern Dharwar craton, having undergone pervasive melting, plutonism and deformation at 2.56–2.50 Ga, and the Western Dharwar craton, which was already relatively stiff at that time, as partly cratonized by 2.61 Ga [*Jayananda et al.*, 2006; *Chardon et al.*, 2008] (see also, for geochronology of the Eastern Dharwar craton, *Friend and Nutman* [1991]) [*Peucat et al.*, 1993; *Jayananda et al.*, 2000; *Vasudev et al.*, 2000; *Chadwick et al.*, 2001, 2007; *Chardon et al.*, 2002; *Rogers et al.*, 2007] (Figure 1).

[7] The study area is located in the Eastern Dharwar craton between the charnockite front, in the south, and the northern tip of the main mass of the Closepet batholith, in the north (Figure 1). This area encompasses a crustal level corresponding to ca. 9 to 18 km paleodepth in the Neoarchean orogen [see *Hansen et al.*,

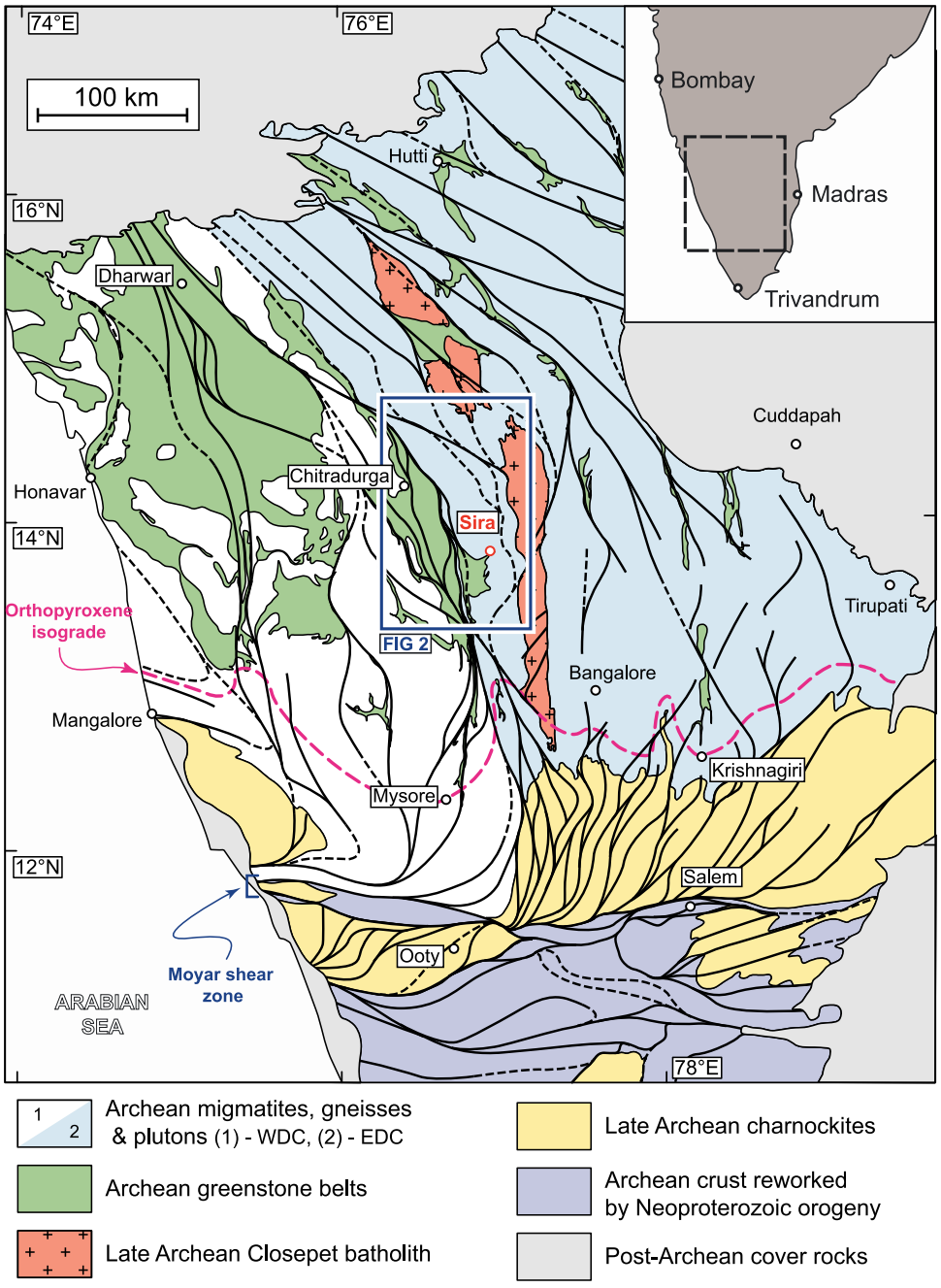

Figure 1. Structural map of the Dharwar craton adapted from *Chardon et al.* [2008]. Shear zones or shear zone boundaries are shown as black lines. As a result of post-Archean northward tilt and consecutive differential erosion, lower levels of the Neoarchean orogen are progressively exposed toward the Moyar shear zone. The Closepet batholith is the only late Archean (2.55–2.51 Ga) magmatic body mapped with confidence so far, but large areas of the Eastern Dharwar craton expose late Archean plutonic complexes. WDC, Western Dharwar craton; EDC, Eastern Dharwar craton.

1984, *Raase et al.*, 1986]. The crust comprised between the Chitradurga greenstone belt and the Closepet batholith (Figure 1) preserves remarkable flat gneissic foliations that are involved in kilometer-scale open lobate synforms trending at a low angle to the eastern branch of the Chitradurga shear zone system (Figure 2). The synforms are occupied by hornblende biotite gneisses (called hereafter the Sira Gneiss complex, SGC) with strong LS tectonites, their mineral-

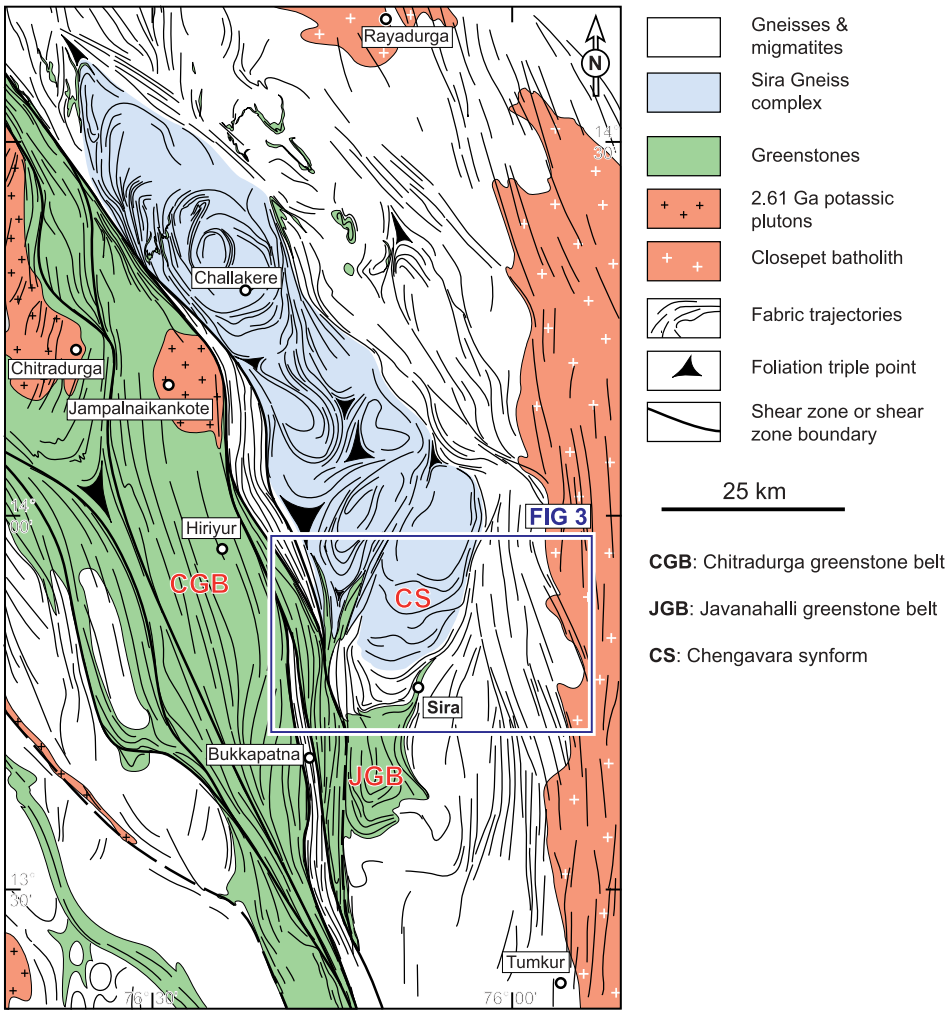

Figure 2. Structural map of the central part of the Dharwar craton showing fabric trajectories and the Chitradurga shear zone system, as well as the approximate extend of the Sira Gneiss complex. The map is based on the photointerpretation of 20 m resolution SPOT multispectral images and field reconnaissance. The frame of the map is located on Figure 1.

stretching lineations trending generally at a low angle to the axes of the synforms.

3. Structure, Kinematics, and Plutonism of the Sira Area

[8] Our work concentrates on a key area of 40 × 20 km around Sira town (Figure 2). This area allows investigating the development of the shallow fabrics of the synforms of SGC as well as their relationships with the underlying Javanahalli greenstone belt and adjoining gneisses, the Chitradurga shear zone system and the Closepet batholith (Figure 2).

3.1. Geology and Overall Structure

[9] The SGC occupies the two NNE trending southernmost synforms of the folded domain mapped on Figure 2. The limbs of the synforms coincide with pinched off digitations of the Javanahalli greenstone belt (Figure 3a). The belt consists of metabasalts and amphibolites preserving HT-LP metamorphic assemblages at 0.4 ± 0.1 GPa and ca. 550°C, as well as arkosic paragneisses and subordinate banded iron formations, quartzites, and calc-silicate rocks [*Naqvi et al.*, 1980; *Seshadri et al.*, 1981; *Narayana et al.*, 1983]. East of Huyildore, the greenstone belt is involved in the Chengavara synform, whereas west of Huyildore, the greenstones are taken into the eastern branch of the Chitradurga shear zone system (Figure 3). The SGC and underlying gneisses of the Chengavara synform are intruded by the Maddakkanahalli plutons (Figure 3). The study area comprises a regional warp of the eastern branch of the Chitradurga shear zone system (Figures 2 and 3a). The southern, N striking segment of the warp hosts the "Bukkapatna

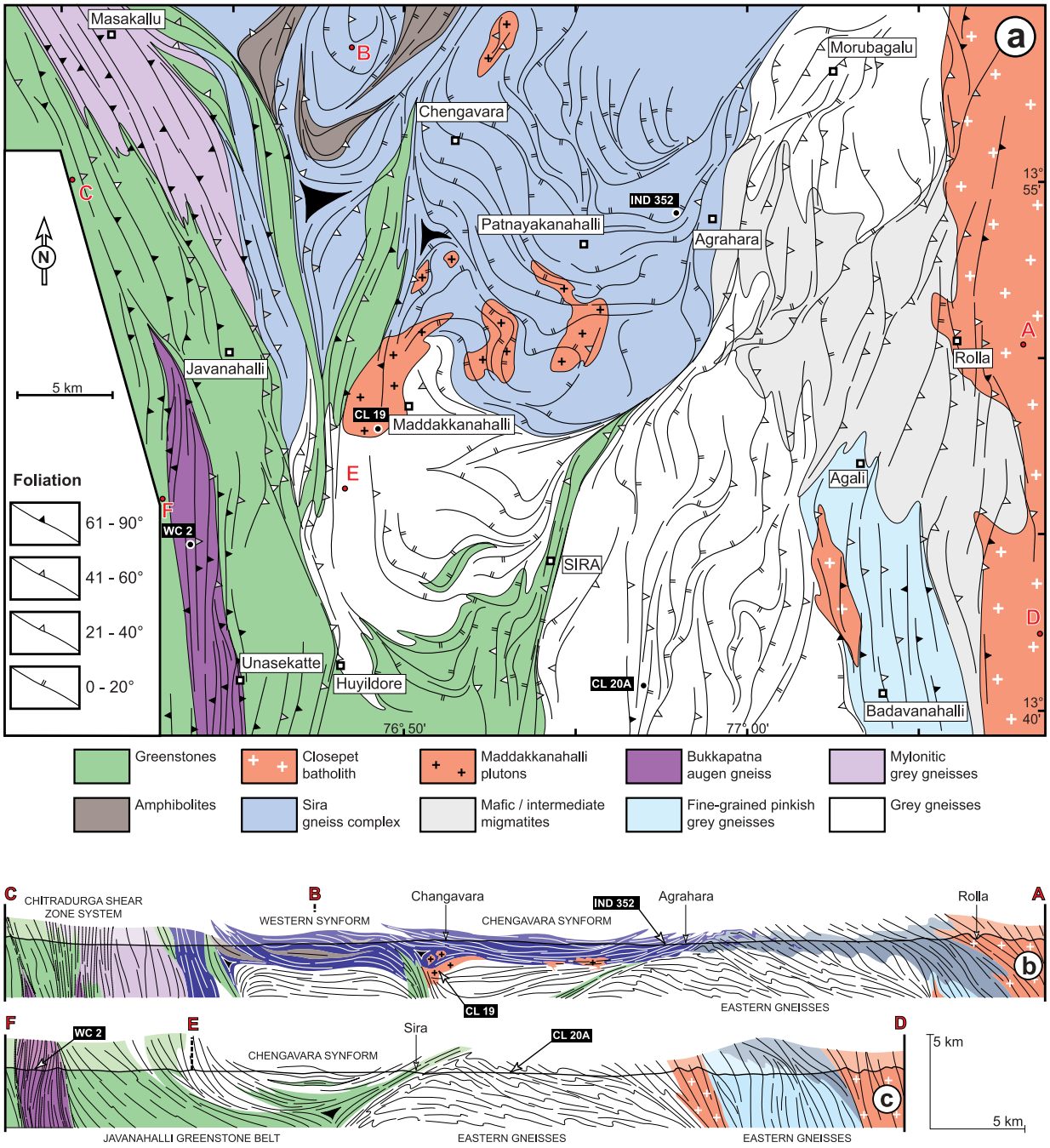

Figure 3. (a) Geology and foliation trajectory map of the Sira area. Foliation measurements are reported on Figure A1 (Appendix A). Geochronological samples are shown by a solid dot and a black label. The frame of the map is located on Figure 2. (b and c) Synthetic cross sections of the area. The lines of section are indicated on the map in Figure 3a by capital letters.

granite" [*Seshadri et al.*, 1981], which actually consists in a steep sheet of mylonitic orthogneiss that tapers off at the latitude of Javanahalli (Figures 2 and 3). The migmatites and gneisses comprised between the Chengavara synform and the Closepet batholith are called hereafter the eastern gneisses (Figure 3). The Closepet batholith is made of comagmatic monzogranites and quartz-monzonites with U-Pb zircon ages of 2518 ± 5 Ma [*Jayananda et al.*, 1995].

3.2. Sira Gneiss Complex: Lobate Synforms

[10] The SGC consists of banded hornblende biotite gneisses showing various degrees of migmatization.

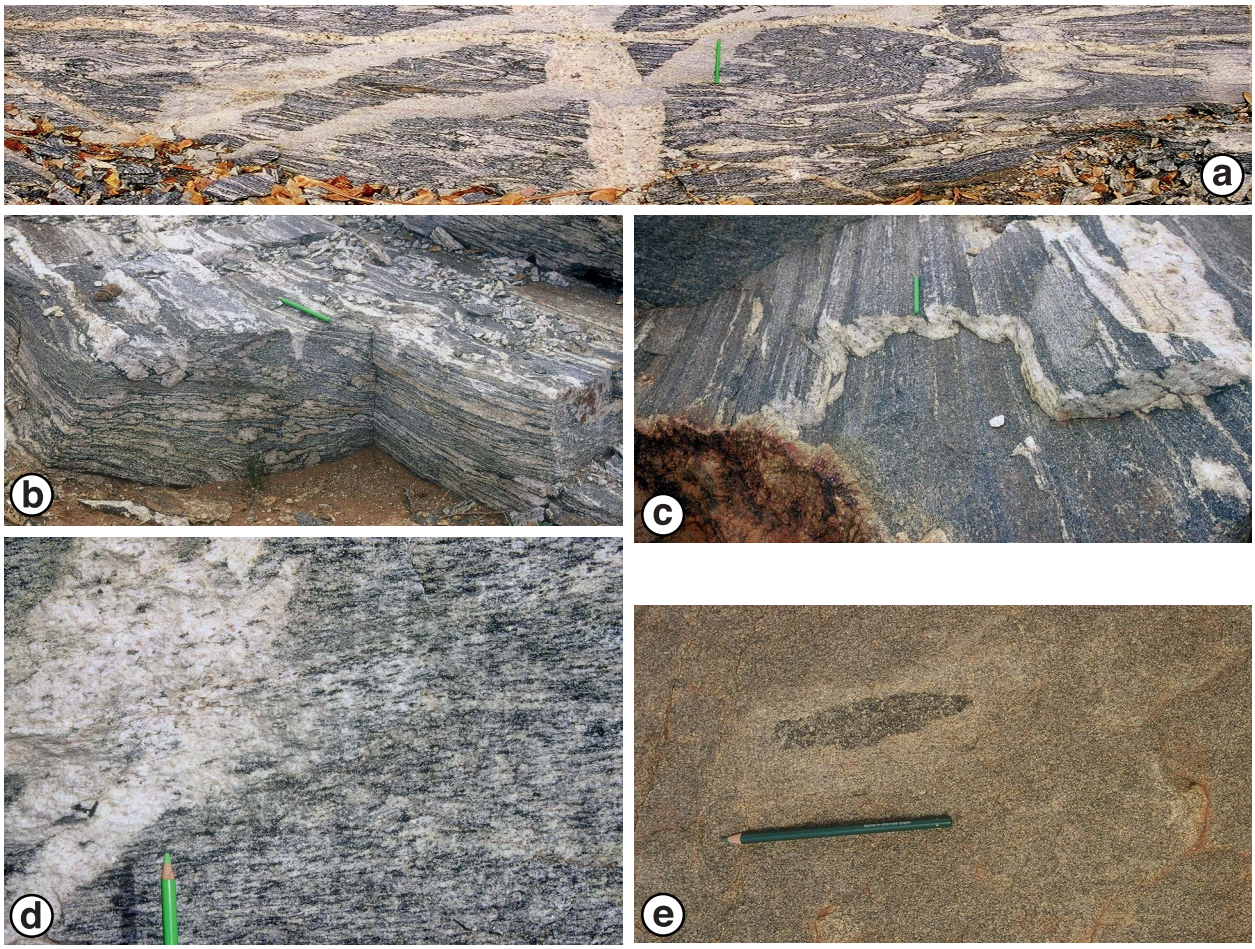

Figure 4. Fabric patterns in the Sira Gneiss complex (see Figure 3a for cited localities). (a) Relations among migmatitic foliation and various generations of veins, the latest and less deformed ones being the pegmatites and the fine-grained biotite tonalite dikes shallowly dipping to the left. Earlier veins show intense folding (XZ section of the strain ellipsoid; vicinity of Chengavara). (b) Three-dimensional view of LS fabrics and ptygmatic folds of veins, vicinity of Chengavara. (c) L > S tectonites marked by a folded biotite tonalite vein. (d) Foliation affecting both sequent hornblende biotite tonalite vein and its host gneiss, 5 km NE of Chengavara (XZ section). (e) Plane view of flat foliation in a Maddakkanahalli intrusion showing a stretched enclave (XY section) trending parallel to the stretching lineation in the surrounding Sira gneiss complex (midway between Chengavara and Maddakkanahalli). Green pencil is for scale.

The SGC hosts a myriad of tonalite veins, which are commonly connected with the leucosomes in the gneiss (Figures 4a and 4b). The entire SGC is characterized by strong subhorizontal L > S and subordinate S = L tectonites (Figures 4b and 4c). The mineral-stretching lineation (L_1), trending dominantly NE, is marked by meter-long rods of quartzofeldpathic aggregates, commonly resulting from folding or transposition of veins (Figures 4c and 5). The tonalite veins emplaced during a protracted period of deformation of the SGC at a time the gneisses were partially molten (Figure 4). Be they sequent or concordant with respect to the gneissic foliation, the veins are either fabric free (Figure 4a) or affected by the same foliation as that of the host gneiss (Figure 4d). Folding of the veins is ubiquitous, whereas boudinage is barely documented (Figures 4a and 4b). Axial surfaces of folds parallel the flat foliation of the host gneisses and their axes trend parallel to the L_1 lineation (Figures 4a to 4c). Folded boudins of veins are rare in the SGC, whereas boudinaged folds are observed, indicating a single deformation episode instead of superimposed strains [*Ramsay*, 1967]. The monotony of the strong L > S and L = S tectonites indicates that deformation was homogeneous at the scale of the SGC and resulted from intense horizontal stretching and vertical shortening, combined with horizontal shortening perpendicular to the stretching direction. No unequivocal macroscopic shear criteria were documented in the SGC,

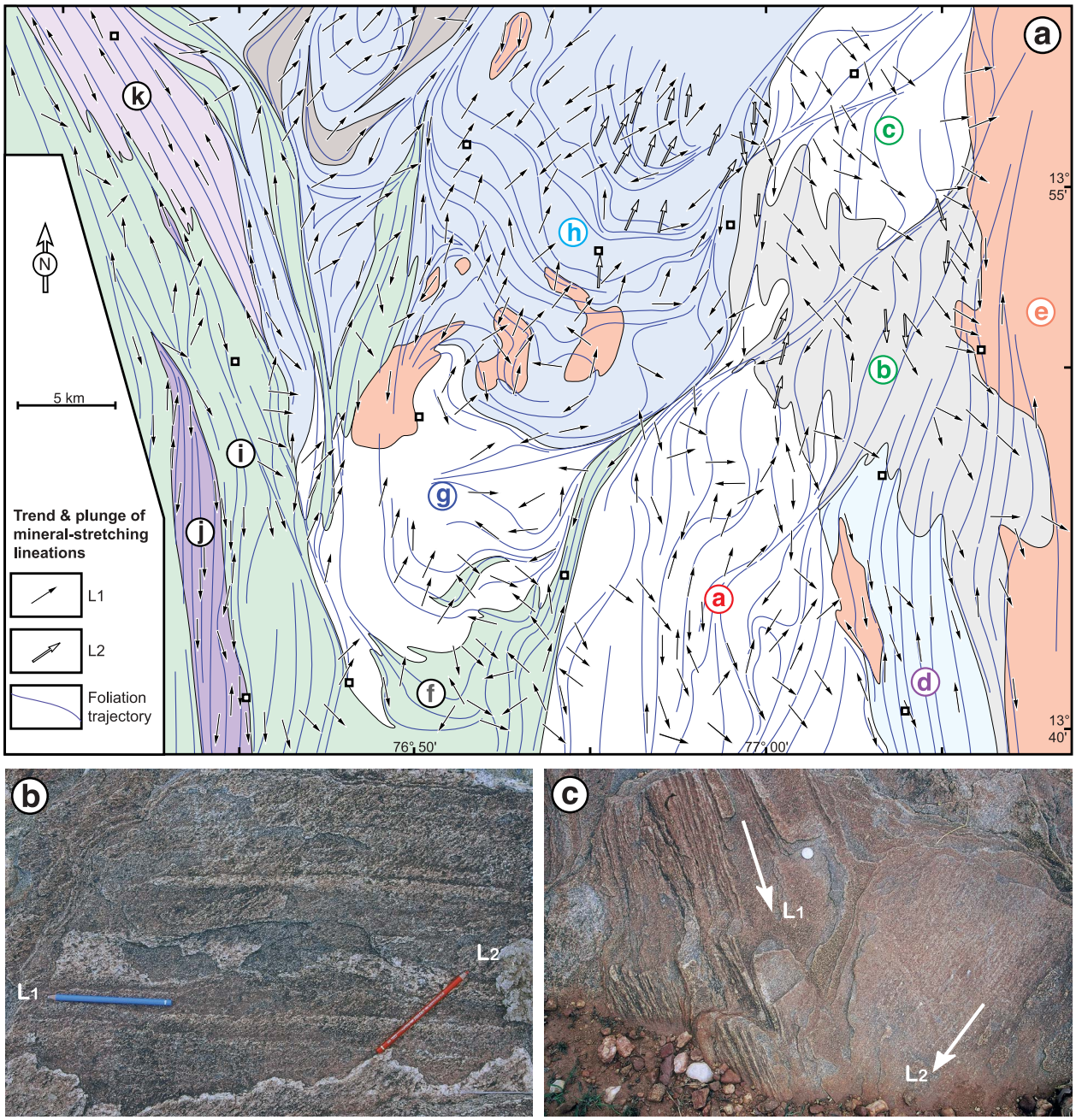

Figure 5. (a) Mineral-stretching lineations of the Sira area plotted on the foliation trajectory map. Letters a to k define the units for which structural measurements are presented in Appendix A. Open squares are locations from Figure 3a. (b) Superimposed mineral-stretching lineations (shown by each pencil) on flat foliation in the Sira gneiss complex (locality of sample IND 352, Figure 3a). (c) Superimposed mineral-stretching lineations on moderately east dipping foliation in the eastern gneisses (unit b), 7 km NNW of Rolla (Figure 3a). Coin is for scale.

arguing for a predominance of coaxial flow during deformation.

[11] The Maddakkanahalli plutons are fine-grained and aplitic granites. The fabric in the plutons may be marked by a diffuse compositional banding, the preferential orientation of biotite crystals, and strained mafic enclaves (Figure 4e). Most parts of the plutons have developed LS fabrics parallel to those of their host SGC gneisses (Figures 3, 4a, and 5). The small intrusions have steeper foliations than those of their host SGC gneisses (Figure 3a), whereas parts of the plutons are devoid of visible fabric or banding. These observations indicate that

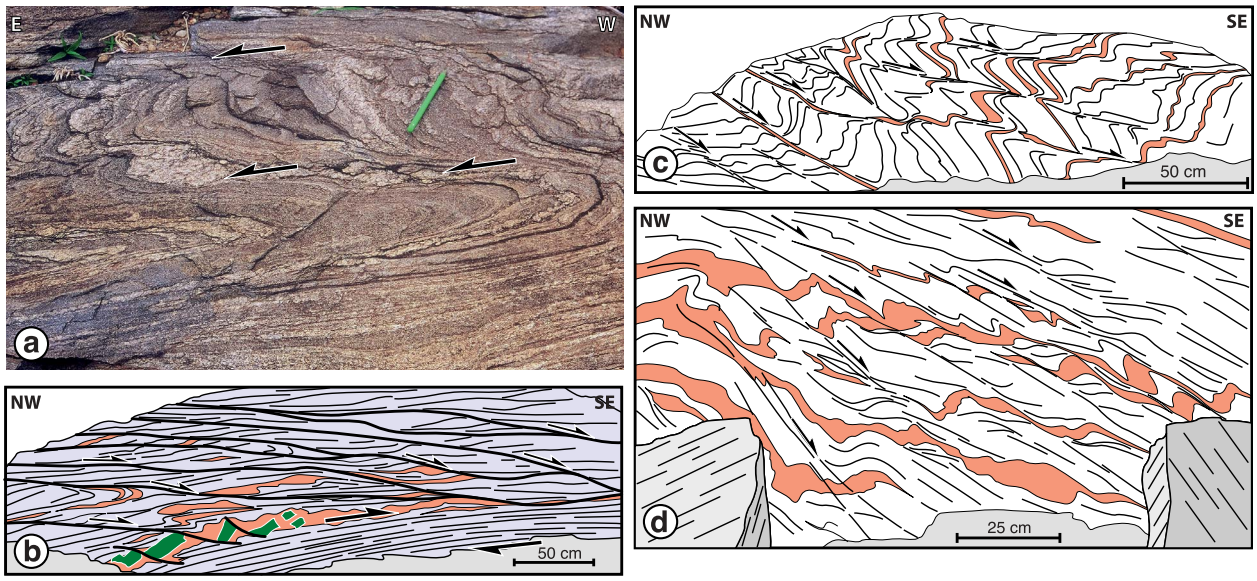

Figure 6. Fold and shear patterns in the eastern gneisses. (a) Similar folds in unit b, 3 km north of Rolla. (b) Low-angle synmelt shear zones in unit b, between Agrahara and Agali (on the trace of a map-scale NE trending shear zone; Figure 5). (c) Relations between folds and shear zones, unit a, 5 km west of Agali. (d) Shear bands and related folds in fabric-free leucocratic veins, unit a (locality of sample CL20A). Leucozomes or granitic veins or felsic gneissic layers are shown in red and amphibolites in green. Sketches are line drawings of field photographs. See Figures 3 and 5 for locations and terminology of the units.

the Maddakkanahalli plutons are synkinematic to late kinematic with respect to the development of the flow fabrics in the SGC.

[12] At the base and below the SGC, rocks of the Chengavara synform have lineations trending at a low angle to the sheared limbs of the synform as well as lineations trending NW or NE (Figure 5a). The bottom of the synform results from transposition of an underlying, steep N-S striking foliation of the greenstone belt (Figure 3c and field observations).

[13] NW of Agrahara, a mineral lineation is superimposed on the L_1 lineation of the SGC (Figure 5). This lineation, called L_2, is marked by the preferential orientation of biotite and hornblende crystals and feldspar aggregates (Figure 5b). L_2 lineations trend parallel to the axial trace of the Chengavara synform (Figure 5). Foliation of the SGC becomes folded on a meter scale approaching the eastern limb of the synform (Figure 3b). First expressed as upright open undulations parallel to the L_2 lineation, these folds become tighter and westerly overturned entering the eastern gneisses.

3.3. Eastern Gneisses

[14] The lower ensemble of the eastern gneisses comprises TTG-type gneisses bearing shallowly east dipping foliations and mineral-stretching lineations plunging NNE to SSE (unit a) as well as fine-grained constrictive gneisses (unit d) with steeply east dipping foliations and shallow lineations (Figures 3c and 5). The upper ensemble of the eastern gneisses is characterized by migmatites and gneisses (units b and c) bearing a moderately east dipping foliation and a downdip L_1 mineral-stretching lineation (Figures 3 and 5). Unit b contains meter-scale to decameter-scale lenses of partially molten SGC gneisses, while unit c hosts large lenses of SGC gneisses in its western part. Field observations at the transition between the SGC and unit b suggest that the SGC intruded unit b before partial melting of both units (Figures 3b and 5). Development of the LS tectonites in the upper ensemble took place at a time partial melting conditions prevailed in unit b. This is attested by a migmatitic foliation and a mineral-stretching lineation comparable to that developed in the SGC (Figures 5b and 5c). A mineral lineation is superimposed on L_1 in unit b (Figure 5c). As the latest fabric developed in the migmatites, this lineation is comparable in nature and orientation to the L_2 lineation documented in the SGC and is therefore considered as the same one in the two rock units (Figure 5).

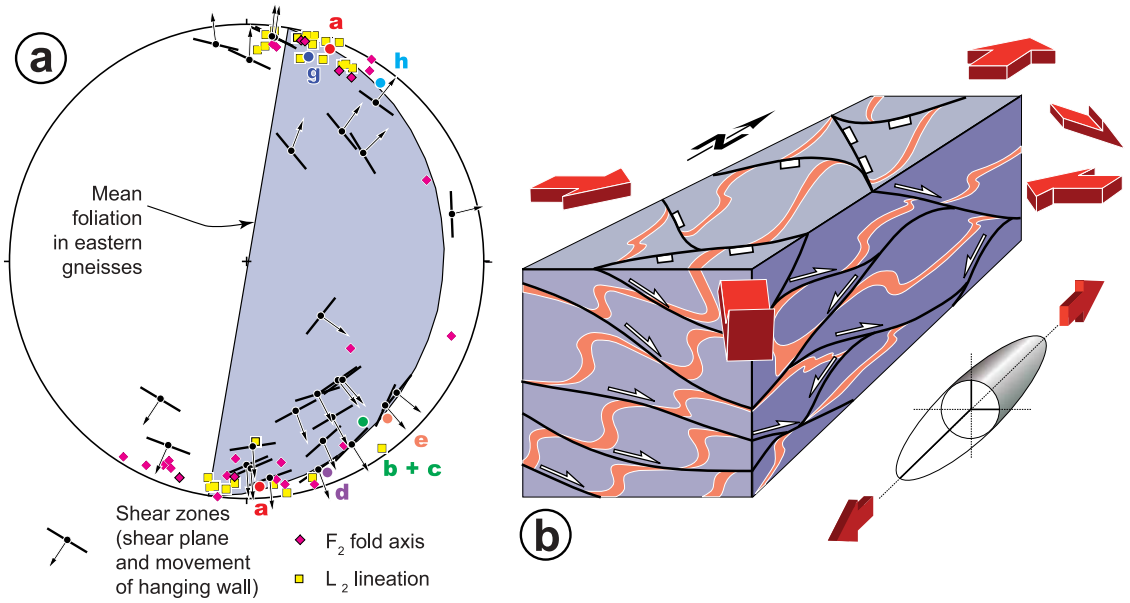

Figure 7. (a) Structural elements in the gneissic rocks located to the east of the Chitradurga shear zone system. Letters a to h refer to the units defined in Figure 5 (see Appendix A for the source of the data). Lower hemisphere, equal area projection. (b) Sketch summarizing the relations between F_2 folding and extensional shearing. Folds may have initially formed as upright folds that have acquired their asymmetry by back rotation along the two sets of extensional shear zones.

[15] The systematic shallow and moderately easterly dipping foliation pattern of the eastern gneisses, particularly in units a and b, reflects pervasive folding on a decimeter to decameter scale. The folds (called F_2) are overturned toward the west and have NNE trending, subhorizontal axes coaxial with L_2 lineations (Figures 6 and 7a). On a majority of outcrops, the fold pattern is intimately linked to a series of extensional shear zones dipping NE or SE (Figures 6 and 7). The backlimbs of the folds are generally attenuated and taken into the shear planes, while their overturned limbs are thick and dip steeper than the shear zones' planes. This configuration indicates that the folds record back rotation of the migmatitic layering between parallel shear planes [*Harris*, 2003]. In migmatitic rocks, the extensional shear zones host foliated or fabric-free tonalites connected with the leucosomes from the overturned limbs of the folds (Figure 6), indicating activation of the shear zones and back rotation of the migmatitic layering under partial melting conditions.

[16] Foliation trajectories in the Chengavara synform and the eastern gneisses evidence oblique, shallowly dipping map-scale shear zones trending NNE and NE (Figures 3a and 5). The NNE trending Sira shear zone coincides with the eastern limb of the Chengavara synform and the Sira greenstone arm, which is beveled between the SGC and the eastern gneisses (Figure 5). The NE trending shear zones deflect the Sira shear zone, and some of them terminate by flanking synformal lobs inside the SGC (Figure 5). One notes the reversal of apparent slip of these shear zones in map view (Figure 5).

3.4. Closepet Batholith and Chitradurga Shear Zone

[17] Along the western margin of the Closepet batholith, the foliation dips shallowly to steeply to the east, parallel to that of the eastern gneisses (Figures 3 and 5). The foliations acquire steeper eastern dips inside the batholith toward the east (Figures 3b and 3c). There is also a concordance between the foliations in the wall rocks and inside the batholith along the eastern margin of the batholith, and the foliation in the eastern country rocks acquire shallow eastern dips further to the east [*Chardon and Jayananda*, 2008]. The mineral lineations in the batholith plunge dominantly in the southeastern quadrant (Figure 5). To the east of the batholith, the east dipping gneissic foliation is affected by a network of melt-bearing extensional shear zones comparable to those of

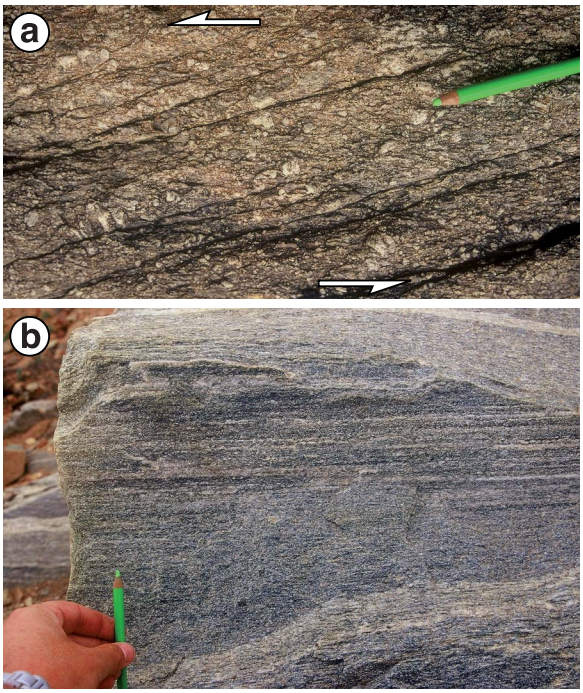

Figure 8. Fabric patterns along the eastern branch of the Chitradurga shear zone system (units j and k, Figure 5). (a) Plane view of Bukkapatna augen gneiss showing brittle-ductile sinistral C′ shear bands (locality of sample WC 2, Figure 3a). Foliation (striking N) and shear bands (striking NNW) are vertical; stretching lineations and slickensides are horizontal. (b) Vertical mylonitic gneiss bearing horizontal stretching lineation (2 km SW of Masakallu, Figure 3a). C′ shear bands and sigma porphyroclasts on this outcrop indicate sinistral shearing. Grain size reduction in Figure 8b and brittle-ductile shear bands in Figure 8a are indicative of lower amphibolite to mostly greenschist facies metamorphic conditions during shearing [*Gapais*, 1989].

the SE dipping set of shears affecting the eastern gneisses (Figure 7).

[18] Along the eastern branch of the Chitradurga shear zone system, i.e., west of Huyildore, greenstones and gneisses acquire a steep foliation and a shallowly plunging stretching lineation (Figures 3 and 5). The Bukkapatna mylonitic gneiss sheet shows pervasive C′ sinistral shear bands, which are particularly well documented in lower-strain lenses of augen gneiss (Figure 8a). The gneisses of unit k (Figure 5) have strong LS tectonites and display sinistral kinematic indicators (Figure 8b).

3.5. Kinematic Synthesis

[19] The above analysis points to a coeval and common kinematic framework for the activation of all the planar and linear fabrics, folding and extensional shearing during overall N-S stretching in the Sira area (Figure 9). L_2 lineations and F_2 folds, which are common to the eastern gneisses and the SGC, as well as the extensional shear zones, imply horizontal directions of stretching that are undistinguishable from those of the L_1 regional stretching lineations (Figure 7a). The constrictional deformation of the SGC, as well as the regional lobate synforms and the F_2 folds attest to the interference of transverse and vertical shortening. The obliquity of the slip vectors of the extensional shear zones on the main stretching direction is indicative of transtensional kinematics during regional deformation (Figure 9b), which is also consistent with constrictional strain [e.g., *Dewey et al.*, 1998]. The kinematic compatibility and geometrical linkage among all the structural elements developed under partial melting is interpreted as the result of a bulk lateral flow process produced by the interplay of strike-perpendicular shortening and transtension during orogen-parallel constrictional stretching (Figure 9c).

[20] The regional deflection of gneissic foliations toward the Closepet batholith in cross-section view (down warping along its western margin and upwarping along its eastern margin) suggests that batholith emplacement was enhanced by transtension with an east side down component of slip. This is consistent with the kinematics of the extensional shear zones documented on both sides of the batholith, pointing to the kinematic and temporal link between lateral crustal flow, transtension, and batholith emplacement (Figure 9a).

4. U-Pb Geochronology

[21] In order to constrain the age and duration of crustal flow and regional strike-slip shearing in the Sira area, we have performed in situ SIMS zircon U-Pb dating of the SGC, the Maddakkanahalli plutons, the eastern gneisses, and the Bukkapatna augen gneiss.

4.1. Results

[22] Sample IND 352 of the SGC (13° 54.33′N, 76° 58.13′E) is a quartz-monzonitic gneiss devoid of evidence of partial melting. Zircons are mainly euhedral and display a visible zoning (Figure 10a). The eight results obtained are concordant to subconcordant and define an intercept at 2559 ± 4 Ma (MSWD = 0.92) and an average $^{207}Pb/^{206}Pb$ age of

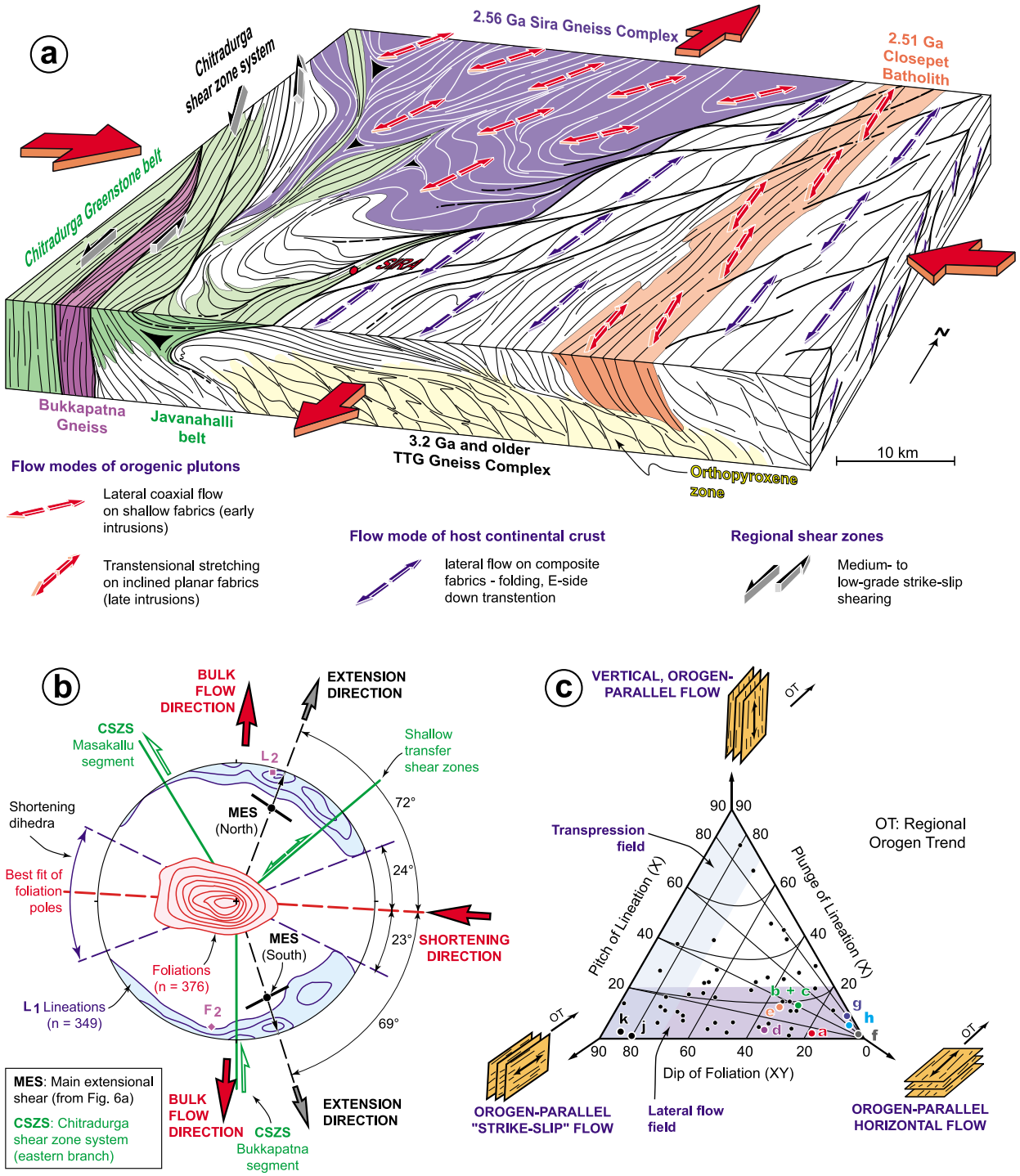

Figure 9. (a) Kinematic framework of crustal flow in the Sira area between 2.56 and 2.50 Ga. Thin lines are traces of foliation and thick lines are shear zones or shear zone boundaries. Flow is assisted and partitioned through a network of partly connected transfer surfaces comprising the oblique map-scale shear zones and the Chitradurga shear zone system. (b) Kinematic synthesis. Contoured data comprise measurements from units a to h (Figures 5 and A1) (1% area contours with contours interval of 2%; lower hemisphere, equal area projection). (c) Fabric data plotted in the crustal flow mode diagram of *Chardon et al.* [2009] (after a plot concept of *Balé and Brun* [1989]). Color-filled circles and letters refer to units defined in Figure 5. Black dots are data from unit i (Figure 5), which extend beyond the lateral flow field (see Appendix A). This is consistent with the greenstones having undergone interference between lateral flow and 2.56–2.50 transpression, and/or preserving inherited steep fabrics.

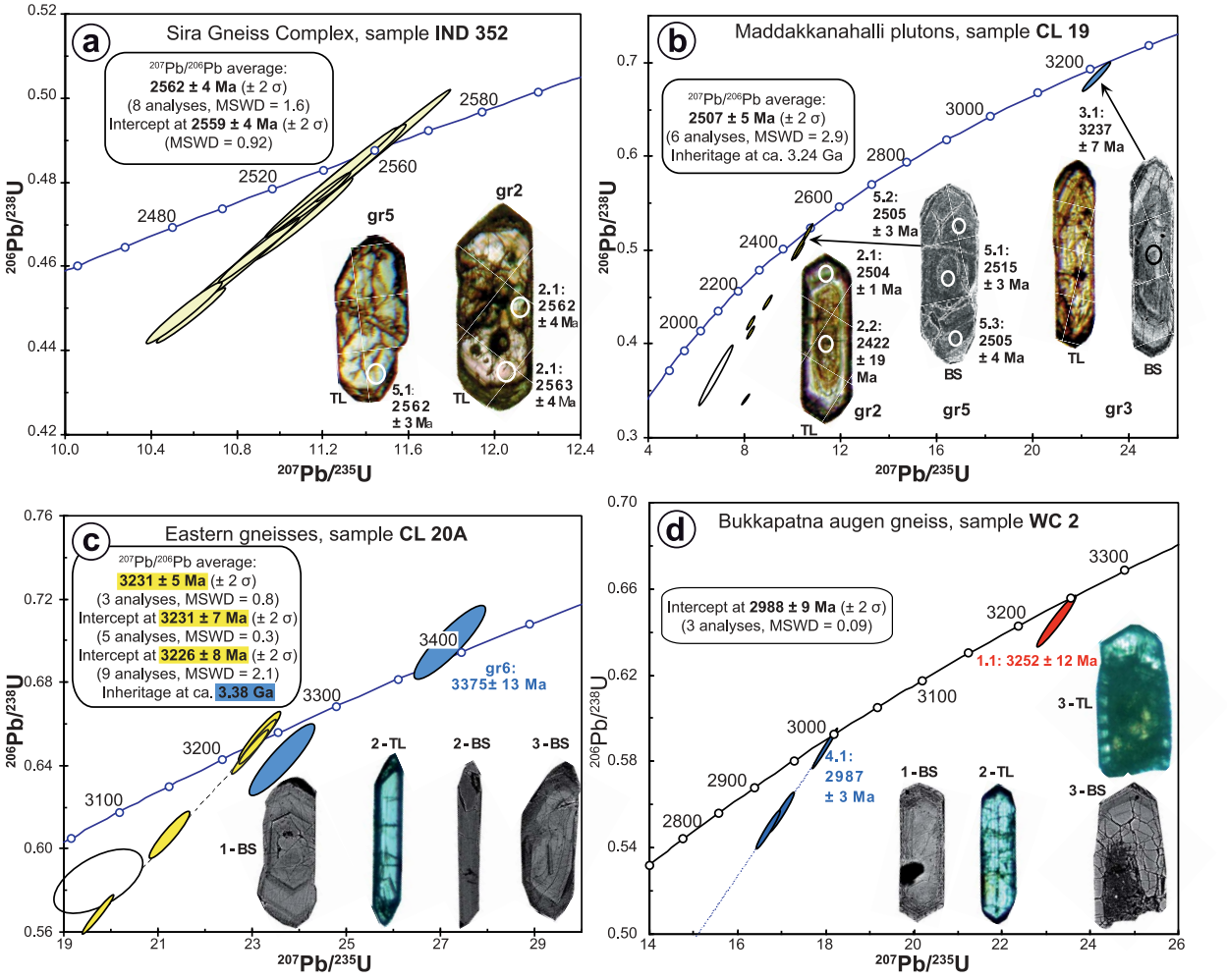

Figure 10. Zircon U-Pb concordia plots for selected rock units of the Sira area. (a and b) These are 1270 CAMECA SIMS data. (c and d) SHRIMP data. TL, transmitted light; BS, backscattered image. Images for samples CL 20A and WC 2 were obtained on grains that were not those used for the SHRIMP analyses. See Table 1 for details. Samples are located on Figure 3.

2562 ± 4 Ma (MSWD = 1.6) (Figure 10a). This age of 2.56 Ga is interpreted as that of the quartz-monzonitic magmatism. Nd model age for this sample is of 2.86 Ga and its ε_{Nd} ratio at 2.56 Ga is of −1. This may indicate a nonnegligible crustal residence time for the source of the SGC. But the slightly negative ε_{Nd} value more likely reflects mixing between a 2.56 Ga subjuvenile source and melt(s) derived from an old (i.e., >3.0 Ga) basement (see below).

[23] Sample CL19 (13° 48.025′N, 76° 49.094′E) is a monzogranitic aplite from the largest of the Maddakkanahalli plutons (Figure 3). Zircons are elongate, euhedral and zoned. Some grains exhibit visible cores (Figure 10b). Zircons are U rich and some analyses are very discordant (grains 7 and 8; Table 1 and Figure 10b). A set of 6 analyses of zoned grains (grains 1, 2.1, 5.1, 5.2, 5.3, 7; Table 1) provides a $^{207}Pb/^{206}Pb$ mean age of 2507 ± 5 Ma (MSWD = 2.9), which is interpreted as that of the crystallization stage of the pluton (Figure 10b). A core (grain 3) is subconcordant with a $^{207}Pb/^{206}Pb$ age of 3237 ± 7 Ma, which is interpreted as an inherited component (Figure 10b).

[24] Sample CL 20A (13° 40.467′N, 76° 57.069′E) is a tonalitic-granodioritic gneiss from unit a devoid of granitoid veins (Figures 3a and 5). A first prominent set of zircons is made of clear and elongate grains (photos 1 and 2; Figure 10c), some with visible concentric zoning (photo 1; Figure 10c). These zircons are interpreted as magmatic. The second set of grains displays cores interpreted as

Table 1. Summary of SHRIMP and SIMS U-Pb Zircon Results[a]

Grain	Spot	U (ppm)	Th (ppm)	Th/U	Pb* (ppm)	$^{204}Pb/^{206}Pb$	Radiogenic Ratios $^{206}Pb/^{238}U$	±	$^{207}Pb/^{235}U$	±	$^{207}Pb/^{206}Pb$	±	r	Ages (Ma) $^{206}Pb/^{238}U$	±	$^{207}Pb/^{206}Pb$	±	Conc. %
Sample IND 352 (Sira Gneiss Complex)																		
1.1		170	268	1.6	69	0.000009	0.469	0.009	11.02	0.20	0.1704	0.0023	0.992	2480	38	2561	4	97
2.1		148	132	0.9	57	0.000018	0.449	0.005	10.55	0.11	0.1705	0.0026	0.970	2391	21	2562	4	93
2.2		183	268	1.5	72	0.000013	0.459	0.008	10.79	0.20	0.1705	0.0023	0.992	2435	37	2563	4	95
3.1		136	139	1.0	52	0.000016	0.448	0.004	10.58	0.10	0.1712	0.0020	0.979	2388	19	2569	3	93
5.1		212	172	0.8	89	0.000013	0.489	0.009	11.48	0.21	0.1704	0.0016	0.996	2565	38	2562	3	100
6.1		272	259	1.0	110	0.000020	0.471	0.007	11.10	0.16	0.1709	0.0026	0.983	2488	29	2567	4	97
7.1		163	194	1.2	67	0.000022	0.481	0.009	11.28	0.20	0.1701	0.0029	0.987	2531	37	2559	5	99
8.1		232	204	0.9	96	0.000022	0.480	0.009	11.24	0.20	0.1698	0.0019	0.995	2527	38	2556	3	99
Sample CL19 (Maddakkanahalli Plutons)																		
1.1		122	129	1.06	38	0.000034	0.363	0.005	8.27	0.11	0.1653	0.0002	0.992	1994	22	2512	2	79
2.1		632	67	0.11	214	0.000053	0.394	0.005	8.95	0.13	0.1651	0.0001	0.997	2143	25	2504	1	86
2.2		874	70	0.08	237	0.000183	0.316	0.021	6.84	0.47	0.1589	0.0018	0.986	1772	104	2422	19	73
3.1	(core)	208	198	0.95	113	0.000038	0.635	0.010	22.64	0.38	0.2585	0.0011	0.962	3171	41	3237	7	98
4.1		1260	702	0.56	247	0.000058	0.228	0.003	4.41	0.06	0.1409	0.0001	0.997	1324	15	2231	2	59
5.1		138	61	0.44	2	0.000012	0.450	0.006	10.27	0.13	0.1654	0.0003	0.989	2393	26	2515	3	95
5.2		101	33	0.33	41	0.000028	0.469	0.006	10.66	0.14	0.1646	0.0003	0.988	2480	27	2505	3	99
5.3		98	36	0.37	38	0.000018	0.452	0.009	10.26	0.19	0.1643	0.0003	0.993	2404	38	2505	4	96
6.1		1388	194	0.14	445	0.000016	0.373	0.005	8.27	0.11	0.1609	0.0002	0.993	2043	23	2465	3	83
7.1		1091	295	0.27	75	0.000260	0.080	0.001	1.82	0.03	0.1677	0.0003	0.976	495	7	2507	4	20
8.1		837	431	0.52	209	0.000045	0.291	0.004	8.07	0.10	0.2014	0.0002	0.995	1647	18	2835	2	58
Sample CL20A (Eastern Gneisses)																		
1.1		1240	23	0.02	199	0.000284	0.186	0.002	4.12	0.06	0.1607	0.0008	0.929	1099	13	2463	9	45
2.1		873	129	0.15	335	0.000018	0.447	0.005	15.00	0.17	0.2436	0.0008	0.958	2381	22	3144	5	76
3.1		1059	23	0.02	242	0.000196	0.265	0.003	7.35	0.13	0.2007	0.0024	0.742	1518	18	2832	19	54
4.1		639	78	0.12	355	0.000022	0.647	0.007	22.96	0.26	0.2576	0.0007	0.973	3215	28	3232	4	99
5.1		704	145	0.21	344	0.000017	0.568	0.006	19.74	0.22	0.2519	0.0007	0.969	2901	25	3197	4	91
6.1	(core)	58	33	0.57	35	0.000164	0.699	0.012	27.19	0.51	0.2821	0.0024	0.895	3417	44	3375	13	101
7.1		213	68	0.32	49	0.001618	0.263	0.003	9.19	0.15	0.2534	0.0026	0.780	1505	17	3206	16	47
7.2		893	86	0.10	337	0.000474	0.436	0.005	14.56	0.18	0.2420	0.0013	0.899	2335	21	3133	8	75
8.1		692	38	0.05	230	0.001129	0.382	0.004	11.92	0.15	0.2264	0.0012	0.898	2084	20	3027	9	69
9.1		1195	160	0.13	271	0.001980	0.257	0.003	6.77	0.22	0.1909	0.0058	0.379	1475	16	2750	50	54
9.2		1379	44	0.03	218	0.000469	0.183	0.002	3.74	0.06	0.1484	0.0013	0.817	1082	13	2328	15	46

Table 1. (continued)

Grain Spot	U (ppm)	Th (ppm)	Th/U	Pb* (ppm)	$^{204}Pb/^{206}Pb$	Radiogenic Ratios						r	Ages (Ma)				Conc. %
						$^{206}Pb/^{238}U$	±	$^{207}Pb/^{235}U$	±	$^{207}Pb/^{206}Pb$	±		$^{206}Pb/^{238}U$	±	$^{207}Pb/^{206}Pb$	±	
10.1	592	91	0.15	332	0.000020	0.652	0.007	23.13	0.26	0.2575	0.0007	0.969	3234	28	3231	4	100
10.2	434	71	0.16	99	0.000080	0.264	0.003	8.10	0.12	0.2223	0.0014	0.894	1512	18	2997	10	50
11.1	1608	226	0.14	210	0.000100	0.152	0.002	2.84	0.04	0.1357	0.0007	0.930	913	11	2173	9	42
11.2	207	7	0.03	108	0.000180	0.607	0.007	21.25	0.28	0.2541	0.0012	0.932	3057	30	3210	8	95
12.1 (core)	61	29	0.47	34	-	0.643	0.011	23.64	0.46	0.2667	0.0022	0.902	3200	44	3287	13	97
13.1	1194	105	0.09	482	0.000300	0.467	0.005	15.03	0.16	0.2332	0.0006	0.970	2473	22	3074	4	80
14.1	1205	342	0.28	290	0.000195	0.280	0.005	7.94	0.14	0.2061	0.0014	0.920	1589	23	2875	11	55
15.1	805	65	0.08	411	0.001338	0.584	0.010	19.72	0.62	0.2448	0.0064	0.556	2967	42	3151	42	94
16.1	581	251	0.43	183	0.000254	0.364	0.005	11.81	0.18	0.2351	0.0010	0.961	2003	25	3087	7	65
17.1	245	181	0.74	138	0.000040	0.654	0.008	23.17	0.30	0.2568	0.0011	0.946	3245	31	3227	7	101
Sample CW2 (Bukkapatna Augen Gneiss)																	
1.1	212	145	0.68	80	0.000566	0.434	0.005	12.82	0.15	0.2141	0.0009	0.935	2325	22	2937	7	79
2.1	747	15	0.02	225	0.000071	0.350	0.004	10.31	0.11	0.2139	0.0007	0.955	1932	17	2935	5	66
3.1	823	348	0.42	202	0.000049	0.285	0.003	7.52	0.08	0.1915	0.0005	0.968	1616	15	2755	4	59
4.1	361	490	1.36	182	0.000046	0.587	0.006	17.87	0.20	0.2208	0.0005	0.980	2978	26	2987	3	100
5.1	229	179	0.78	62	0.001093	0.308	0.005	8.40	0.16	0.1976	0.0016	0.900	1733	25	2807	13	62
6.1	1183	627	0.53	260	0.000334	0.254	0.004	5.78	0.68	0.1646	0.0192	0.123	1462	19	2504	196	58
7.1 (core)	104	14	0.14	57	0.000005	0.645	0.008	23.20	0.29	0.2609	0.0009	0.957	3209	30	3252	6	99
8.1	312	152	0.49	108	0.000081	0.402	0.005	10.95	0.16	0.1973	0.0015	0.841	2180	22	2804	13	78
9.1	746	332	0.45	179	0.000216	0.278	0.003	6.60	0.07	0.1721	0.0004	0.972	1582	15	2578	4	61
10.1	198	99	0.50	94	0.000227	0.549	0.006	16.57	0.19	0.2188	0.0007	0.957	2822	25	2972	5	95
11.1	295	136	0.46	112	0.000273	0.440	0.005	12.64	0.15	0.2083	0.0009	0.932	2351	21	2893	7	81
12.1	1288	646	0.50	166	0.000235	0.150	0.002	1.98	0.03	0.0960	0.0008	0.774	899	9	1548	16	58
13.1	164	113	0.69	79	0.000111	0.557	0.006	16.87	0.20	0.2195	0.0007	0.957	2856	26	2977	5	96
14.1	937	420	0.45	197	0.000141	0.245	0.003	5.90	0.07	0.1748	0.0007	0.928	1411	13	2604	7	54

[a]Uncertainties are given at the 2σ level; 100% Conc. indicates concordant analysis. Samples IND352 and CL19 were analyzed on IMS1270 (CRPG Nancy). Samples CL20A and CW2 were analyzed on SHRIMP2 (ANU Canberra).

inherited zircons (photo 3; Figure 11c). Magmatic zircons are very rich in U and 13 of the 19 analyses are strongly discordant (Table 1 and Figure 10c). Only three analyses of magmatic zircons are concordant (grains 4, 10.1, 17) and define an average $^{207}Pb/^{206}Pb$ age at 3231 ± 5 Ma (MSWD = 0.8). They also define, together with grains 5 and 11, an intercept age at 3231 ± 7 Ma (MSWD = 0.3). Additionally, four of the discordant analyses fall on the discordia and the age with the 9 analyses is 3226 ± 8 Ma (MSWD = 2.1). The three above calculation types provide coherent results and we retain the age of 3231 ± 5 Ma as that of the magmatic precursor of the gneiss. A core (grain 12) is subconcordant at 3287 ± 13 Ma and a second one (grain 6) exhibits a concordant age at 3375 ± 13 Ma. These ages are interpreted as inherited (Table 1 and Figure 10c).

[25] Sample WC2 (13° 44.739′N, 76° 44.017′E) comes from a decameter-long lense of monzogranitic augen gneiss in the Bukkapatna mylonitic sheet (Figures 3a and 10d). Ten of 14 U-Pb analyses are moderately to strongly discordant (Figure 10d). A set of 3 analyses, corresponding to elongate magmatic zoned zircons (photos 1 and 2, Figure 10d), is concordant to subconcordant and defines an intercept at 2988 ± 9 Ma (MSWD = 0.09) (Table 1 and Figure 10d). Two discordant points fall on this discordia, defining, together with the 3 analyses mentioned above, a similar intercept age at 2988 ± 6 Ma (MSWD = 1.4). Some grains have cores that are generally strongly metamict (photos 3, Figure 10d). One analysis is nevertheless concordant with a $^{207}Pb/^{206}Pb$ age of 3252 ± 6 Ma (Table 1). The age of 2.99 Ga is interpreted as that of the monzogranite precursor of the Bukkapatna gneiss and that of 3.25 Ga as inherited from a preexisting crust.

4.2. Implications of the U-Pb Data

[26] Magmatic crystallization of the SGC took place at 2559 ± 4 Ma, providing a maximum age for the initiation of lateral flow of the SGC. Flow lasted until 2507 ± 5 Ma, as constrained by the U-Pb zircon age of the Maddakkanahalli plutons, which crystallized during the latest increments of flow of the SGC. There is an intimate link between partial melting and the development of the shears, folds and fabrics recording lateral flow of the eastern gneisses, the SGC and the SGC lenses enclosed in the eastern gneisses. Therefore, partial melting and associated flow of the 3.23 Ga eastern gneisses took place essentially after 2559 ± 4 Ma, i.e., the crystallization age of the SGC. Pervasive crustal flow between 2559 ± 4 Ma and 2507 ± 5 Ma is consistent with the 2.518 ± 5 Ma U-Pb age of the Closepet batholith, which emplaced during flow.

[27] The 2988 ± 6 Ma age of the Bukkapatna augen gneiss sets a poorly constrained upper bound to the slip history of the eastern branch of the Chitradurga shear zone system. But as the latest active and coldest structure in the study area (Figure 8), the shear zone was obviously active after 2560 Ma (age of the SGC) and probably until after 2507 ± 5 Ma (age of the Maddakkanahalli plutons). The 3237 ± 7 Ma age obtained on a zircon core from the Maddakkanahalli pluton indicates assimilation or partial melting of a 3.23 Ga old basement that was most likely the eastern gneisses, dated at 3231 ± 5 Ma. Finally, the magmatic (3.00, 3.23 Ga) and inherited (3.25, 3.27, 3.37 Ga) dates obtained from pre–2.56 Ga gneisses argue for discrete magmatic pulses between 3.37 and 3.00 Ga.

5. Lateral Constrictional Flow: Definition and Implications for Neoarchean Orogeny in South India

[28] Between 2.56 and 2.50 Ga, the lower crust of the Eastern Dharwar craton underwent pervasive, three-dimensional flow process that we suggest to call lateral constrictional flow (LCF). LCF combines orogen-parallel constrictional stretching and symmetrical transtension with respect to the main flow direction (Figure 9). Flow was absorbed by early syntectonic plutons (SGC, 2.56 Ga) by pure shear dominated deformation producing lobate gneissic sills aligned in the direction of flow. The transtensional component of flow assisted intrusion of late kinematic elongate plutons (Closepet, 2.51 Ga) in the direction of horizontal flow (Figure 9). In the pre–2.56 Ga crust, flow activated a composite fabric by folding, orogen parallel stretching and transtensional shearing, all coeval and kinematically compatible with fabrics developed in 2.56–2.50 Ga intrusions (Figures 7 and 9). The heterogeneity of the LCF pattern on a map scale tends to be absorbed by a three-dimensional network of slip surfaces such as the shallow transfer zones and the regional strike-slip shear zones (Figure 9a).

[29] Our analysis shows that overturned folds in high-grade terrains may be misleading indicators of thrusting. Indeed, although they attest to shortening normal to their axes, folds may acquire their asymmetry by back folding between extensional shears in a context of horizontal flow at a shallow angle to their axes (Figure 7). Westward thrusting of the

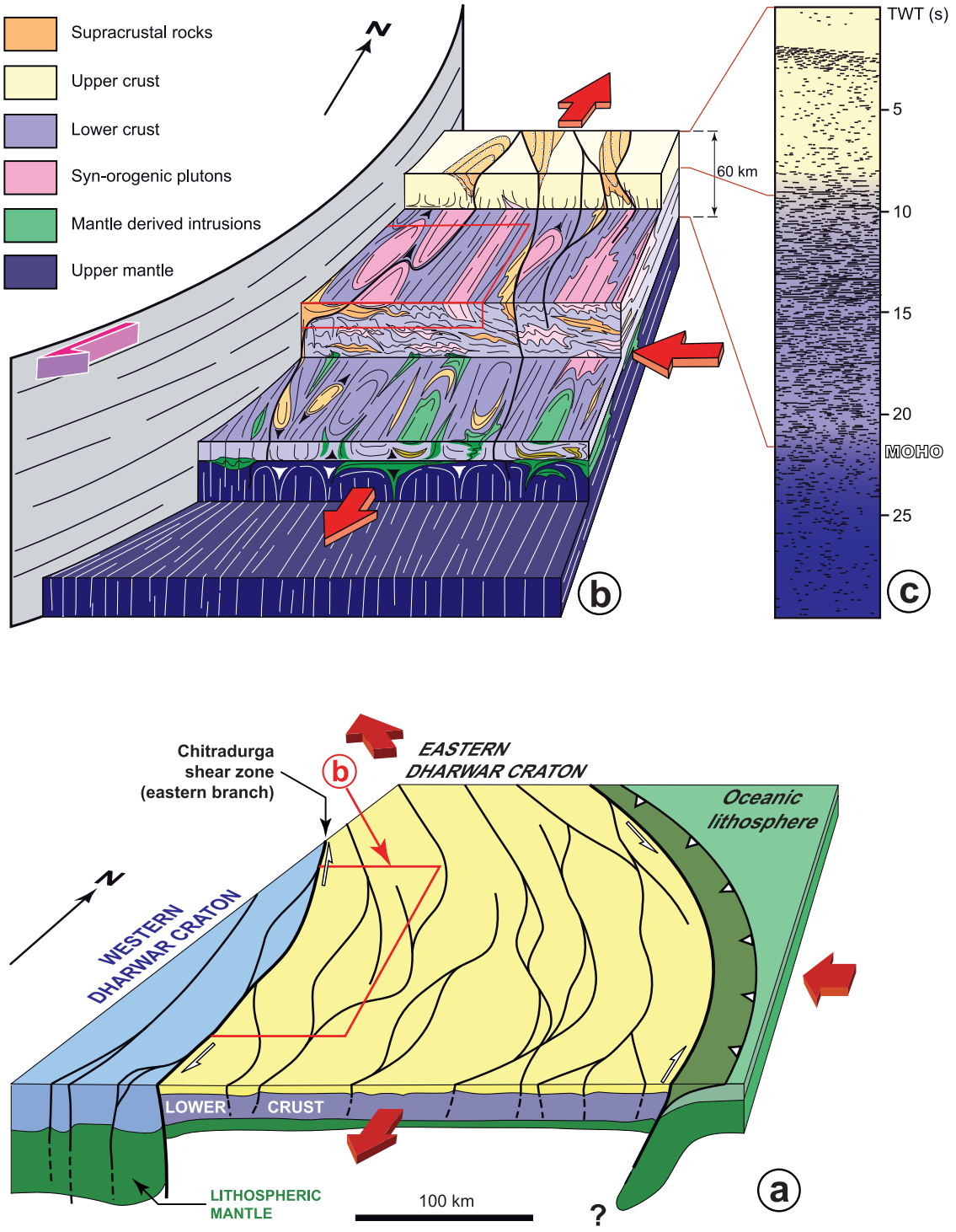

Figure 11. (a) Configuration of the Neoarchean orogen of south India between 2.56 and 2.50 Ga. The eastern edge of the orogen may be tentatively seen as a westward dipping subduction. Transient mechanical decoupling along this subduction could have resulted in synconvergence eastward spreading of the orogen, which would explain the systematic east side down transtensional component of lateral constrictional flow (e.g., Figure 7). (b) Textural and compositional fabric pattern of the central part of the Neoarchean orogen. The red box corresponds to the block diagram of Figure 9a. A tentative comparison is suggested between the crustal texture of the Eastern Dharwar craton and the INDEPTH III reflection seismic data (c) from the Bangoin shot in central Tibet (adapted from *Ross et al.* [2004]).

gneisses and/or the Javanahalli greenstone belt upon the Chitradurga greenstone belt postulated on the basis of fold asymmetry [e.g., *Naqvi et al.*, 1980; *Drury*, 1983] or a west vergent fold-and-thrust belt tectonic model [e.g., *Drury*, 1983; *Chadwick et al.*, 2007] may therefore be precluded. Investigations undertaken south of 15°N [*Chardon et al.*, 2002, 2008; *Chardon and Jayananda*, 2008] that are summarized below attest to the pervasiveness of Neoarchean LCF on a regional scale.

[30] Gneisses and migmatites of the Eastern Dharwar craton bear a shallowly dipping foliation that is variously overprinted by a steeply east dipping foliation. Despite latest strain accumulation on steep fabrics, the flat and steep foliations were activated synchronously over a protracted period of widespread partial melting and plutonism between 2.56 and 2.51 Ga. The regional mineral-stretching lineation trends dominantly N-S at a low angle to the foliations' strike and plunges shallowly. N-S stretching is assisted by synmelt conjugate strike-slip shear zones documented from an outcrop to a craton scale (Figures 1 and 11). Horizontal stretching is also enhanced by synmelt SE dipping extensional shear zones. This, together with the fact that the steep foliation commonly shows apparent east side down strain slip (e.g., Figure 9a), indicates that the eastward transtensional component of flow is widespread in the Eastern Dharwar craton. The greenstone belts are upright synforms elongated in the direction of regional stretching (Figure 1). They preserve steep orogen-parallel foliations bearing lineations with preferentially high pitches. To summarize, regional structural data argue for the interplay of transpression- and/or sagging-dominated deformation of greenstone belts [*Chadwick et al.*, 2000, 2007; *Chardon et al.*, 2008] and LCF at a craton scale in a crust that remained hot, partially molten and therefore potentially thermally buffered for a long time (60 Ma) [see *Depine et al.*, 2008; *Chardon et al.*, 2009] (Figure 11).

[31] LCF responds to boundary conditions imposed to a hot, buoyant and soft crust under convergence by absorbing tectonic shortening and laterally expelling the overthickened crust. The transtensional component of LCF responds to the body forces due to the topographic load and the buoyancy of the lower crust by thinning the orogen in order to maintain a flat Moho. LCF compensates for heterogeneities generated by the redistribution of masses of contrasted densities and viscosities inside the lower crust during convergence. The heterogeneities may be due, for instance, to the incorporation of upper crustal material into the lower crust. LCF also contributes to the mitigation of rheological contrasts or volume changes due to melt production and migrations. To summarize, LCF tends to achieve mechanical, and therefore thermal homogenization of a thick "waterbed" of lower crust under convergence. Therefore, LCF provides a structural mechanism for achieving intracrustal isostatic compensation of topographic relief by lower crustal flow as envisaged by *Bird* [1991]. In other words, LCF is instrumental in maintaining a subdued topography in a hot (i.e., soft) convergent setting. As a complement to LCF as a relief-smoothing agent, sedimentation prevails in cold (i.e., stiff) convergent settings to mitigate relief by filing up large depressions between mountain ranges supported by lithospheric-scale thrusts [*Tapponnier et al.*, 2001].

[32] The properties of LCF exposed above may account for the salient geological characteristics of lower crustal exposures of hot Precambrian orogens, such as (1) horizontal isograds and absence of major reverse metamorphic pressure breaks, suggesting minor topographic gradients, (2) synconvergence HT-LP metamorphism, and (3) dominance of orogen-parallel stretching and transcurrent kinematics [*Cagnard et al.*, 2006b; *Chardon et al.*, 2009; *Gapais et al.*, 2009]. Numerous studies of hot orogens are implicitly or explicitly suggestive of LCF (Precambrian examples: *Ehlers et al.* [1993], *Dirks et al.* [1997], *Passchier et al.* [1997], *Vassallo and Wilson* [2002], *Davis and Maidens* [2003], *Gapais et al.* [2005, 2008], *Cagnard et al.* [2006b], *Nitescu et al.* [2006], *Duclaux et al.* [2007], *Hamilton* [2007], *Dumond et al.* [2010], and *Lana et al.* [2010]; Phanerozoic examples: *Aerden* [1998], *Franke et al.* [2011], *Klepeis and Crawford* [1999], *Andronicos et al.* [2003], and *Denèle et al.* [2007]). LCF is also required to operate in three-dimensional experiments on the shortening of weak lithospheres [*Cagnard et al.*, 2006b; *Cruden et al.*, 2006; *Rey and Houseman*, 2006; *Duclaux et al.*, 2007].

[33] The applicability of LCF to a large variety of hot convergent settings prompts to evaluate its contribution to the deep kinematics and structure of active orogenic plateaux. Indeed, given its width, boundary conditions, and monotony of its HT-LP metamorphic grade, we propose that the Neoarchean orogen of south India (Figure 11a) [*Chardon et al.*, 2008] exposes the type-lower crust that may underlie the Altiplano or Tibet and undergo lateral flow [e.g., *Yang et al.*, 2003; *Royden et al.*, 2008]. In the following, we explore the interactions between LCF, upper crustal faulting and upper mantle flow as coupled structural mechanisms regulating three-

dimensional mass balance in hot convergent orogens, with a reference to the Tibet example.

6. Kinematic and Geophysical Implications for Orogenic Plateaux and Hot Orogens

6.1. Lateral Constrictional Flow and Crustal-Scale Kinematics

[34] Two configurations of LCF may be envisaged in a large hot orogen such as the Tibet-Himalayan system (Figure 12a). Inside the plateau, LCF makes the thick lower crust act as a strain gauge between the upper crust deforming by a combination of shortening and transtension [*Andronicos et al.*, 2007] and the uppermost mantle undergoing lateral flow [*Holt*, 2000] (Figure 12b). Upper crustal deformation is accommodated through a array of conjugate transcurrent faults and N-S striking normal faults, both controlling the formation of sedimentary basins [*Taylor et al.*, 2003; *Murphy et al.*, 2010; *Sanchez et al.*, 2010]. Distributed faulting contributes to homogeneous shortening compensated by diffuse eastward extrusion of the upper crust, suggesting plane strain conditions [*Zhang et al.*, 2004; *Andronicos et al.*, 2007]. The brittle-ductile transition acts as an attachment layer [*Tikoff et al.*, 2002] absorbing the kinematic heterogeneities generated by interference of LCF and upper crustal faulting (Figure 12b). The attachment also accommodates the drag effect of the eastward drifting upper crust onto the lower crust and/or the drag effect of LCF onto the upper crust. Upper mantle fabrics revealed by the birefringence of teleseismic waves are aligned parallel to NE to ENE striking sinistral faults in central Tibet, suggesting coupling of the deformation on a lithospheric scale across the thick lower crust [*Holt*, 2000; *Andronicos et al.*, 2007]. In this setting, LCF acts to maintain the compatibility between horizontal plane strain extrusion of the upper crust and lateral flow of the upper mantle through a thin plateau lithosphere deforming coherently in response to convergence (Figure 12b).

[35] The southern margin of the Tibetan Plateau coincides with the inner and thickest part of the Himalayan collisional wedge (Figure 12a). In such a setting, LCF makes the middle crust act as a strain gauge between lateral collapse of the upper crust and thrust thickening in the lower crust (Figure 12c). Post 15 Ma synconvergence lateral collapse of the upper crust is attested by orogen-normal grabens, orogen-parallel stretching lineations, and metamorphic core complexes associated with orogen-parallel directions of extension [e.g., *Gapais et al.*, 1992; *Murphy and Copeland*, 2005; *Jessup et al.*, 2008; *Kali et al.*, 2010]. Orogen-normal shortening of the upper crust is coeval with lateral extension, and interferes with low-angle strike-slip faulting, which accommodates the obliquity of the convergence. Shortening is marked by shallowly plunging corrugations, upright macroscopic and mesoscopic folds, constrictive fabrics and the preferential elongation of the metamorphic core complexes, all trending at a low angle to the main structural grain [e.g., *Murphy and Copeland*, 2005]. Short-traveled sediments are trapped in intermountain basins bounded by the detachment faults and orogen-parallel thrust ranges [*Saylor et al.*, 2010] (Figure 12c). These basins contribute to smoothing out the topography of the roof of the orogenic wedge by incorporating clastic sediments into the crust, and possibly down into the lower crust (Figure 12c). In this context, the attachment accommodates interference between shortening, strike slip and normal faulting of the upper crust and lateral flow of the lower crust. Additionally, the attachment filters upper crustal material being stuffed down into the lower crust by combined extension, sedimentation and shortening, and that has not been expelled laterally by extension (Figure 12c). The transtensional component of LCF should decrease downward in the crust to account for the reorientation of the X strain axis from orogen parallel in the upper crust (lateral extension) to orogen normal in the lower crust (orogen normal thrusting; Figure 12c). In other words, LCF adapts in space and time to the relative influence or magnitude of gravitational collapse, orogen-normal shortening, and thrust thickening.

[36] LCF in ultrahot orogens, typified by wide Precambrian accretionary orogens, represents a third end-member case illustrated by the Eastern Dharwar craton (Figure 11). In such a context, LCF is pervasive through a particularly thick and fluid lower crust over the entire width of the orogen, and accommodates distributed thickening of the upper crust, preferential downward movement of upper crustal rocks into the lower crust and coupling with distributed flow of the upper mantle [*Chardon et al.*, 2009] (present study). LCF may more generally combine various proportions of the three end-member modes explored here (inner orogenic wedge, plateau interior, and ultrahot orogen) and evolve through time and space in a given convergent setting.

6.2. Seismic Signature of Lateral Constrictional Flow

[37] Foliations are systematically flat or shallowly dipping in the Sira area outside the Chitradurga shear

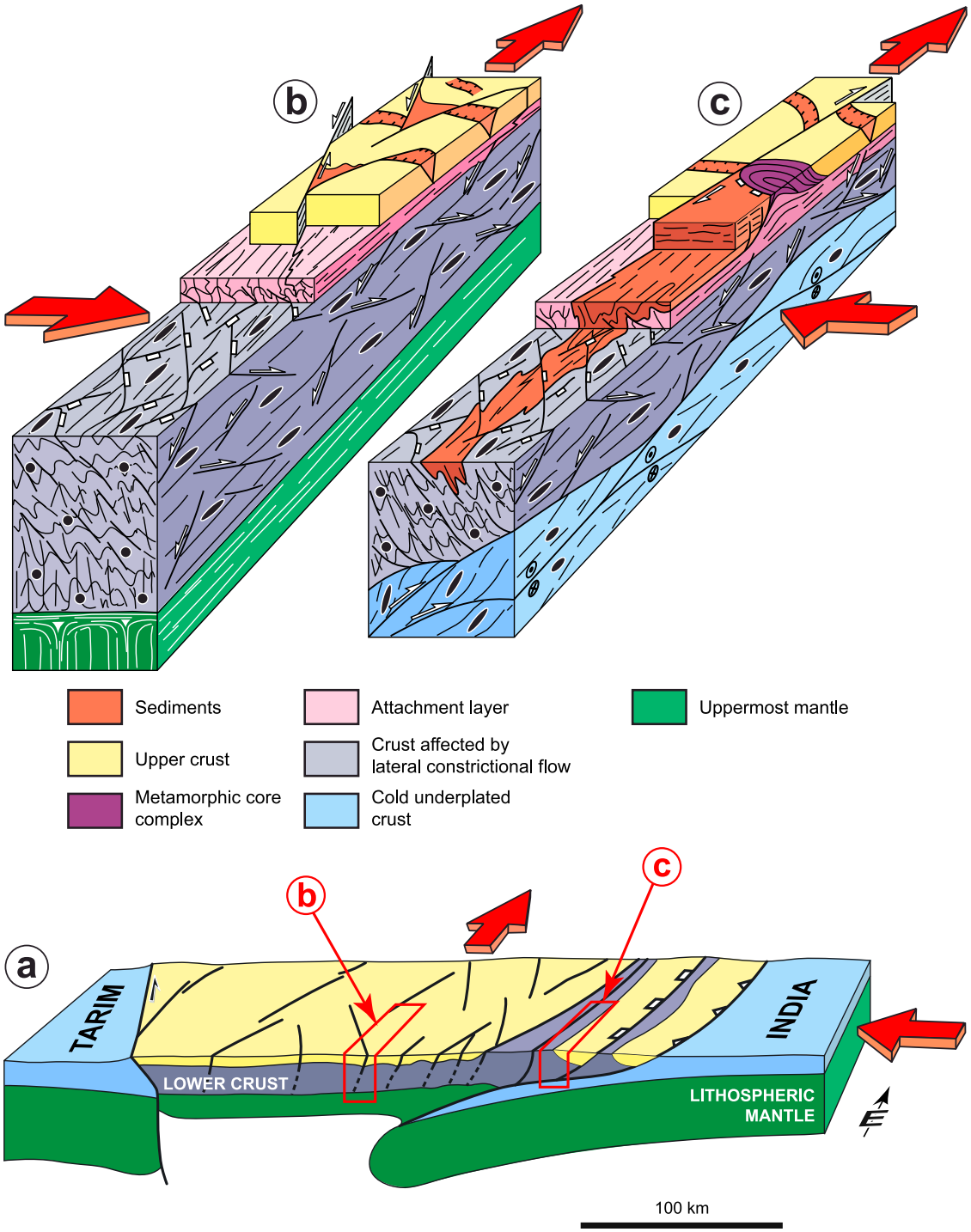

Figure 12. Operative modes of lateral constrictional flow (LCF) in a wide hot orogen bearing a high plateau, with reference to the Tibet example. (a) Sketch block diagram of the Central portion of the Himalayan-Tibet orogenic system. (b) Kinematic relationships between LCF, uppermost mantle flow, and upper crustal deformation in the central part of the plateau. (c) Kinematic relationships between LCF, lower crustal thrust duplex stacking, and lateral collapse of the upper crust in the inner and thickest part of the collisional wedge. Black ellipses represent the principal sections of the strain ellipsoid. The strike-slip (conjugate) shear zone patterns in the lower crust are omitted.

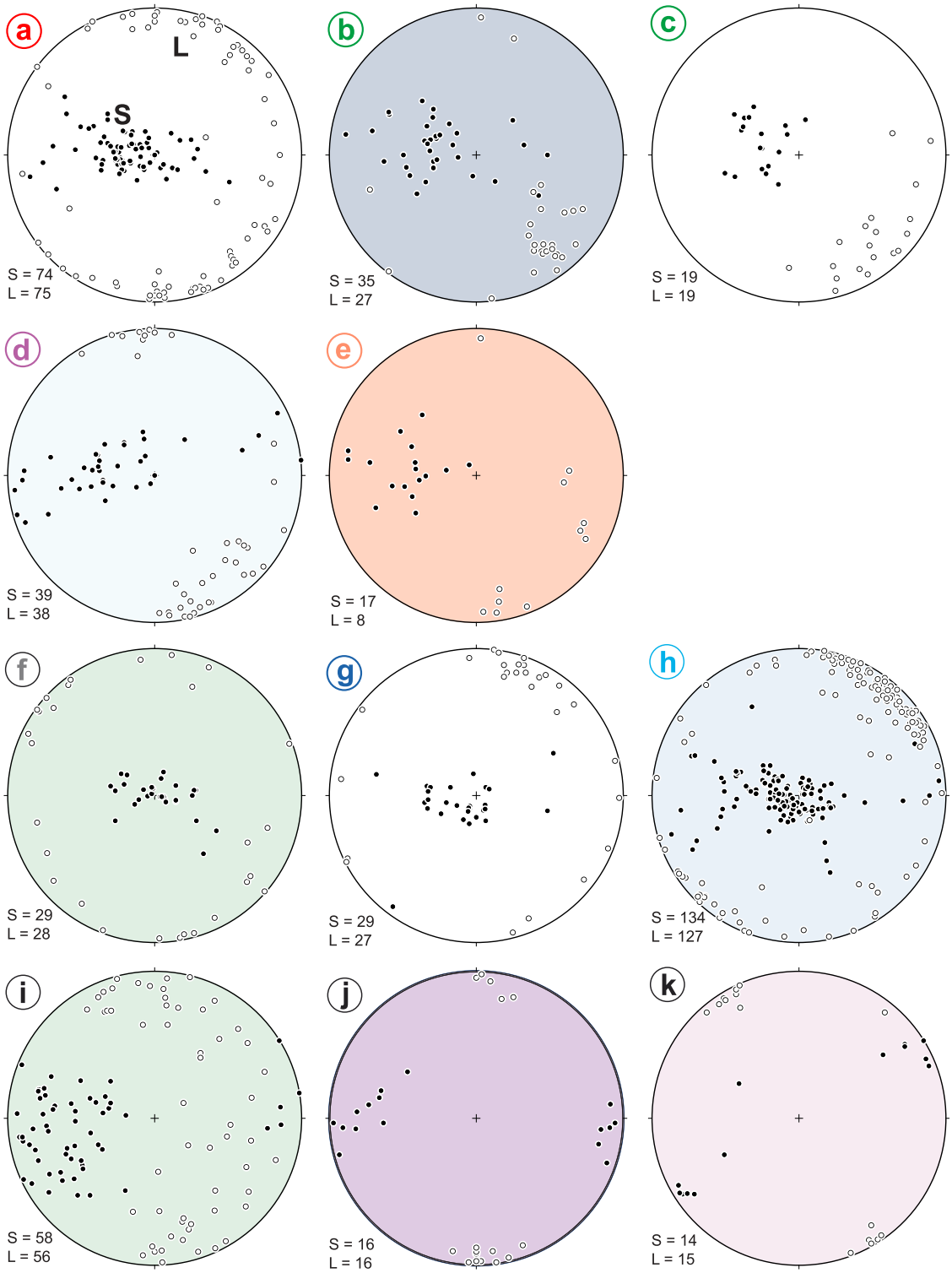

Figure A1. Foliation and L_1 lineation measurements of the study area (lower hemisphere, equal area projection). Open circles are lineations and filled circles are poles to foliations. Letters a to k refer to the map units defined on Figure 5. S, number of foliation measurements; L, number of lineation measurements.

zone system (Figures 3a and 9). The composite foliation pattern in pre–2.56 Ga crustal rocks is linked to macroscopic folding. The enveloping surface of these folds is flat to shallowly dipping, implying that the dip of the foliations was originally shallow. On a metric to decametric scale, these foliations coincide with a compositional lamination made of various gneissic lenses, amphibolites and greenstone slivers of variable degree of partial melting. Such a lamination is further enhanced on a decameter to kilometer scale by the syntectonic magmatic intrusions flattened as horizontal sills and/or elongate in the direction of lateral flow (Figures 3b, 3c, and 9). This layering may be extrapolated to most parts the Eastern Dharwar craton, even where a steep, late foliation has developed [*Chardon and Jayananda*, 2008; *Chardon et al.*, 2008] (Figure 11b).

[38] To summarize, LCF produces a crustal-scale lamination resulting both from reworking of inherited (i.e., pre–2.56 Ga) compositional textures and from the shaping of plutons intruded during 2.56–2.50 Ga LCF (Figure 11b). Laminae of various gneisses, migmatites, amphibolites and supracrustals have contrasted seismic velocities owing to their contrasted compositions, hence providing the impedance contrasts best explaining a strong seismic reflectivity [*Mooney and Meissner*, 1992]. We therefore consider LCF as an alternative to extension, channel flow or even thrusting for producing the thick reflective lower crust of hot orogens such as Tibet [see *Haines et al.*, 2003; *Ross et al.*, 2004] or Precambrian accretionary orogens [*Van Der Velden et al.*, 2006] (Figure 11c).

[39] Importantly, the penetrative orogen-parallel, subhorizontal prolate strain produced by LCF (e.g., Figure 7b) would obviously account for the subhorizontal, orogen-parallel seismic anisotropy of the lower crust such as that measured in central Tibet [*Sherrington et al.*, 2004]. The fact that the seismic anisotropy of the uppermost mantle of central Tibet parallels that of the lower crust and the strike-slip faults reinforces the view that LCF achieves kinematic coherency between coupled crust and the mantle in a hot lithosphere deforming in a convergent setting.

7. Conclusion

[40] The wide crustal transition exposing the Neoarchean orogen of south India allows documenting a pervasive, three-dimensional flow mode of crust, called lateral constrictional flow (LCF). LCF combines orogen-normal shortening, lateral constrictional stretching, and transtension. LCF provides a structural mechanism to absorb gravity-driven flow, lateral escape, and mass redistribution in a thickened viscous crust submitted to convergence. LCF therefore tends to mechanically and thermally homogenize the lower crust and maintain a subdued topography under convergence. Three end-members are envisaged for LCF in type-geodynamic contexts: (1) plateau interiors, (2) inner part of collisional crustal wedges or plateau edges, and (3) throughout wide ultrahot orogens. In these three configurations, LCF makes the lower crust act as a strain gauge between gravitational collapse or tectonic thickening of the upper crust, thrust stacking in the lowermost crust (collisional crustal wedge case), crustal shortening, and flow in the upper mantle. In the case of plateau interiors and ultrahot orogens, LCF achieves coupling of upper crustal deformation with upper mantle flow through a hot and thin lithosphere deforming coherently under convergence. Although fundamentally a three-dimensional tectonic process, LCF generates a lamination that may produce the lower crustal pattern of strong planar reflectivity recorded on orogen-normal reflection seismic lines such as those acquired in Tibet. LCF may also provide a source for the lateral seismic anisotropy of Tibet.

Appendix A: Fabric Measurements and Treatment

[41] Figure A1 shows all the foliation and lineation measurements collected at 440 field stations distributed over the study area (Figures 3a and 5). With the exception of unit i (Figure 5), the data are reasonably clustered for each map unit so that they have been plotted as single points on Figures 7a and 9b from maxima computed on each stereogram of Figure A1.

Acknowledgments

[42] This study was funded by the Indo-French Centre for the Promotion of Advanced Research (IFCPAR project 2307–1). We thank Chris Andronicos, Laurent Jolivet, an anonymous referee, and Thorsten Becker for stimulating reviews and editorial guidance that helped sharpen our arguments and/or improve the readability of the work. We acknowledge the technical staff at the CRPG in Nancy and the ANU in Canberra (PRISE) for invaluable support and help during acquisition of the zircon U-Pb SIMS data. Flora Bajolet contributed to the diagram concept of Figure 12.

References

Aerden, D. (1998), Tectonic evolution of the Montagne Noire and a possible orogenic model for syncollisional exhumation of deep rocks, Variscan belt, France, *Tectonics*, *17*, 62–79, doi:10.1029/97TC02342.

Andronicos, C. L., D. H. Chardon, and L. S. Hollister (2003), Strain partitioning in an obliquely convergent orogen, plutonism, and synorogenic collapse: Coast Mountains Batholith, British Columbia, Canada, *Tectonics*, *22*(2), 1012, doi:10.1029/2001TC001312.

Andronicos, C. L., A. A. Velasco, and J. M. Hurtado (2007), Large-scale deformation in the India-Asia collision constrained by earthquakes and topography, *Terra Nova*, *19*, 105–119, doi:10.1111/j.1365-3121.2006.00714.x.

Balé, P., and J.-P. Brun (1989), Late Precambrian thrust and wrench zones in Northern Brittany (France), *J. Struct. Geol.*, *11*, 391–405, doi:10.1016/0191-8141(89)90017-5.

Beaumont, C., R. A. Jamieson, M. H. Nguyen, and S. Medvedev (2004), Crustal channel flows: 1. Numerical models with applications to the tectonics of the Himalayan-Tibetan orogen, *J. Geophys. Res.*, *109*, B06406, doi:10.1029/2003JB002809.

Bird, P. (1991), Lateral extrusion of lower crust from under high topography, in the isostatic limit, *J. Geophys. Res.*, *96*, 10,275–10,286, doi:10.1029/91JB00370.

Cagnard, F., J. P. Brun, and D. Gapais (2006a), Modes of thickening of analogue weak lithospheres, *Tectonophysics*, *421*, 145–160, doi:10.1016/j.tecto.2006.04.016.

Cagnard, F., N. Durrieu, D. Gapais, J. P. Brun, and C. Ehlers (2006b), Crustal thickening and lateral flow during compression of hot lithospheres, with particular reference to Precambrian times, *Terra Nova*, *18*, 72–78, doi:10.1111/j.1365-3121.2005.00665.x.

Chadwick, B., V. N. Vasudev, and G. V. Hedge (2000), The Dharwar craton, southern India, interpreted as the result of Late Archaean oblique convergence, *Precambrian Res.*, *99*, 91–111, doi:10.1016/S0301-9268(99)00055-8.

Chadwick, B., G. V. Hedge, A. P. Nutman, and V. N. Vasudev (2001), Syenite emplacement during accretion of the Late Archaean Dharwar batholith, south India: SHRIMP U/Pb age and structure of the Koppal pluton, Karnataka, *J. Geol. Soc. India*, *58*, 381–390.

Chadwick, B., V. N. Vasudev, G. V. Hedge, and A. P. Nutman (2007), Structure and SHRIMP U/Pb ziron ages of granites adjacent to the Chitradurga schist belt: Implications for Neoarchaean convergence in the Dharwar craton, southern India, *J. Geol. Soc. India*, *69*, 5–24.

Chardon, D., and M. Jayananda (2008), Three-dimensional field perspective on deformation, flow, and growth of the lower continental crust (Dharwar craton, India), *Tectonics*, *27*, TC1014, doi:10.1029/2007TC002120.

Chardon, D., J. J. Peucat, M. Jayananda, P. Choukroune, and C. M. Fanning (2002), Archean granite-greenstone tectonics at Kolar (south India): Interplay of diapirism and bulk inhomogeneous contraction during juvenile magmatic accretion, *Tectonics*, *21*(3), 1016, doi:10.1029/2001TC901032.

Chardon, D., M. Jayananda, T. R. K. Chetty, and J. J. Peucat (2008), Precambrian continental strain and shear zone patterns: South Indian case, *J. Geophys. Res.*, *113*, B08402, doi:10.1029/2007JB005299.

Chardon, D., D. Gapais, and F. Cagnard (2009), Flow of ultrahot orogens: A view from the Precambrian, clues for the Phanerozoic, *Tectonophysics*, *477*, 105–118, doi:10.1016/j.tecto.2009.03.008.

Cruden, A. R., M. H. B. Nasseri, and R. Pysklywec (2006), Surface topography and internal strain variation in wide hot orogens from three-dimensional analogue and two-dimensional numerical vice models, in *Analogue and Numerical Modelling of Crustal-Scale Processes*, edited by S. J. H. Buiter and G. Schreurs, *Geol. Soc. Spec. Publ.*, *253*, 79–104, doi:10.1144/GSL.SP.2006.253.01.04.

Davis, B. K., and E. Maidens (2003), Archaean orogen-parallel extension: Evidence from the northern Eastern goldfields province, Yilgarn craton, *Precambrian Res.*, *127*, 229–248, doi:10.1016/S0301-9268(03)00189-X.

Denèle, Y., P. Olivier, G. Gleizes, and P. Barbey (2007), The Hospitalet gneiss dome (Pyrenees) revisited: Lateral flow during Variscan transpression in the middle crust, *Terra Nova*, *19*, 445–453, doi:10.1111/j.1365-3121.2007.00770.x.

Depine, G. V., C. L. Andronicos, and J. Phipps-Morgan (2008), Near-isothermal conditions in the middle and lower crust induced by melt migration, *Nature*, *452*, 80–83, doi:10.1038/nature06689.

Dewey, J. F., R. E. Holdsworth, and R. A. Strachan (1998), Transpression and transtension zones, in *Continental Transpressional and Transtensional Tectonics*, edited by R. Holdsworth, R. E. Strachan, and R. A. Dewey, *Geol. Soc. Spec. Publ.*, 135, 1–14, doi:10.1144/GSL.SP.1998.135.01.01.

Dirks, P. H. G. M., J. S. Zhang, and C. W. Passchier (1997), Exhumation of high-pressure granulites and the role of lower crustal advection in the North China Craton near Datong, *J. Struct. Geol.*, *19*, 1343–1358, doi:10.1016/S0191-8141(97)00044-8.

Drury, S. A. (1983), A regional tectonic study of the Archean Chitradurga greenstone belt, Karnataka, based on LANDSAT interpretation, *J. Geol. Soc. India*, *24*, 167–184.

Drury, S. A., and R. W. Holt (1980), The tectonic framework of the south Indian craton: A reconnaissance involving LANDSAT imagery, *Tectonophysics*, *65*, T1–T15, doi:10.1016/0040-1951(80)90073-6.

Duclaux, G., P. Rey, S. Guillot, and R.-P. Ménot (2007), Orogen-parallel flow during continental convergence: Numerical experiments and Archean field examples, *Geology*, *35*, 715–718, doi:10.1130/G23540A.1.

Dumond, G., P. Goncalves, M. L. Williams, and M. J. Jercinovic (2010), Subhorizontal fabric in exhumed continental lower crust and implications for lower crustal flow: Athabasca granulite terrane, western Canadian Shield, *Tectonics*, *29*, TC2006, doi:10.1029/2009TC002514.

Ehlers, C., A. Lindroos, and O. Selonen (1993), The late Svecofenian granite-migmatite zone of southern Finland—A belt of transpressive deformation and granite emplacement, *Precambrian Res.*, *64*, 295–309, doi:10.1016/0301-9268(93)90083-E.

England, P. C., and A. B. Thompson (1984), Pressure temperature time paths of regional metamorphism. 1. Heat transfer during the evolution of regions of thickened continental crust, *J. Petrol.*, *25*(4), 894–928.

Franke, W., M. P. Doublier, K. Klama, S. Potel, and K. Wemmer (2011), Hot metamorphic core complex in a cold foreland, *Int. J. Earth Sci.*, in press.

Friend, C. R. L., and A. P. Nutman (1991), SHRIMP U-Pb geochronology of the Closepet granite and Peninsular gneisses, Karnataka, south of India, *J. Geol. Soc. India*, *38*, 357–368.

Gapais, D. (1989), Shear structures within deformed granites: Thermal and mechanical indicators, *Geology*, *17*, 1144–1147, doi:10.1130/0091-7613(1989)017<1144:SSWDGM>2.3.CO;2.

Gapais, D., A. Pecher, E. Gilbert, and M. Ballevre (1992), Synconvergence spreading of the Higher Himalaya Crystal-

line in Ladakh, *Tectonics*, *11*, 1045–1056, doi:10.1029/92TC00819.

Gapais, D., A. Potrel, and N. Machado (2005), Kinematics of long-lasting Paleoproterozoic transpression within the Thompson Nickel Belt, Manitoba, Canada, *Tectonics*, *24*, TC3002, doi:10.1029/2004TC001700.

Gapais, D., A. Pelletier, R.-P. Ménot, and J.-J. Peucat (2008), Paleoproterozoic tectonics in the Terre Adélie craton (East Antarctica), *Precambrian Res.*, *162*, 531–539, doi:10.1016/j.precamres.2007.10.011.

Gapais, D., F. Cagnard, F. Gueydan, P. Barbey, and M. Ballevre (2009), Mountain building and exhumation processes through time: Inferences from nature and models, *Terra Nova*, *21*, 188–194, doi:10.1111/j.1365-3121.2009.00873.x.

Haines, S. S., S. L. Klemperer, L. Brown, G. R. Jingru, J. Mechie, R. Meissner, A. Ross, and W. J. Zhao (2003), INDEPTH III seismic data: From surface observations to deep crustal processes in Tibet, *Tectonics*, *22*(1), 1001, doi:10.1029/2001TC001305.

Hamilton, W. B. (2007), Earth's first two billion years—The era of internally mobile crust, *Mem. Geol. Soc. Am.*, *200*, 233–296, doi:10.1130/2007.1200(13).

Hansen, E. C., R. C. Newton, and S. Janardhan (1984), Pressures, temperatures and metamorphic fluids across an unbroken amphibolite facies to granulite facies transition in southern Karnataka, India, in *Archaean Geochemistry*, edited by A. Kröner, G. N. Hanson, and A. M. Goodwin, pp. 160–181, Springer, Berlin.

Harris, L. B. (2003), Folding in high-grade rocks due to back-rotation between shear zones, *J. Struct. Geol.*, *25*, 223–240, doi:10.1016/S0191-8141(02)00024-X.

Holt, W. E. (2000), Correlated crust and mantle strain fields in Tibet, *Geology*, *28*, 67–70, doi:10.1130/0091-7613(2000)28<67:CCAMSF>2.0.CO;2.

Jayananda, M., H. Martin, J. J. Peucat, and B. Mahabaleswar (1995), Late Archean crust-mantle interactions: Geochemistry of LREE-enriched mantle derived magmas. Example of the Closepet Batholith, southern India, *Contrib. Mineral. Petrol.*, *119*(2–3), 314–329.

Jayananda, M., J.-F. Moyen, H. Martin, J.-J. Peucat, B. Auvray, and B. Mahabaleswar (2000), Late Archaean (2550–2520 Ma) juvenile magmatism in the Eastern Dharwar craton, southern India: Constraints from geochronology, Nd-Sr isotopes and whole rock geochemistry, *Precambrian Res.*, *99*, 225–254, doi:10.1016/S0301-9268(99)00063-7.

Jayananda, M., D. Chardon, J. J. Peucat, and R. Capdevila (2006), 2.61 Ga potassic granites and crustal reworking in the Western Dharwar craton (India): Tectonic, geochronologic and geochemical constraints, *Precambrian Res.*, *150*, 1–26, doi:10.1016/j.precamres.2006.05.004.

Jayananda, M., T. Kano, J. J. Peucat, and S. Channabasappa (2008), 3.35 Ga komatiite volcanism in the western Dharwar craton, southern India: Constraints from Nd isotopes and whole-rock geochemistry, *Precambrian Res.*, *162*, 160–179, doi:10.1016/j.precamres.2007.07.010.

Jessup, M. J., D. L. Newell, J. M. Cottle, A. L. Berger, and J. A. Spotila (2008), Orogen-parallel extension and exhumation enhanced by denudation in the trans-Himalayan Arun River gorge, Ama Drime Massif, Tibet-Nepal, *Geology*, *36*, 587–590, doi:10.1130/G24722A.1.

Kali, E., P. H. Leloup, N. Arnaud, G. Maheo, D. Y. Liu, E. Boutonnet, J. Van der Woerd, X. H. Liu, L. Z. Jing, and H. B. Li (2010), Exhumation history of the deepest central Himalayan rocks, Ama Drime range: Key pressure-temperature-deformation-time constraints on orogenic models, *Tectonics*, *29*, TC2014, doi:10.1029/2009TC002551.

Klemperer, S. L. (2006), Crustal flow in Tibet: Geophysical evidence for the physical state of Tibetan lithosphere, and inferred patterns of active flow, in *Channel Flow, Ductile Extrusion and Exhumation in Continental Collision Zones*, edited by R. D. Law, M. P. Searle, and L. Godin, *Geol. Soc. Spec. Publ.*, 268, 39–70, doi:10.1144/GSL.SP.2006.268.01.03.

Klepeis, K. A., and M. L. Crawford (1999), High-temperature arc-parallel normal faulting and transtension at the roots of an obliquely convergent orogen, *Geology*, *27*, 7–10.

Lana, C., A. Kisters, and G. Stevens (2010), Exhumation of Mesoarchean TTG gneisses from the middle crust: Insights from the Steynsdorp core complex, Barberton granitoid-greenstone terrain, South Africa, *Geol. Soc. Am. Bull.*, *122*(1–2), 183–197, doi:10.1130/B26580.1.

Meissner, R., W. Rabbel, and H. Kern (2006), Seismic lamination and anisotropy of the lower continental crust, *Tectonophysics*, *416*, 81–99, doi:10.1016/j.tecto.2005.11.013.

Mooney, W. D., and R. Meissner (1992), Multi-genetic origin of crustal reflectivity: A review of seismic reflection profiling of the continental lower crust, in *Continental Lower Crust*, edited by D. M. Fountain, R. J. Arculus, and R. W. Kay, pp. 45–79, Elsevier, Amsterdam.

Murphy, M. A., and P. Copeland (2005), Transtensional deformation in the central Himalaya and its role in accommodating growth of the Himalayan orogen, *Tectonics*, *24*, TC4012, doi:10.1029/2004TC001659.

Murphy, M. A., V. Sanchez, and M. H. Taylor (2010), Syncollisional extension along the India-Asia suture zone, south-central Tibet: Implications for crustal deformation of Tibet, *Earth Planet. Sci. Lett.*, *290*(3–4), 233–243, doi:10.1016/j.epsl.2009.11.046.

Naqvi, S. M., B. L. Narayana, P. Rama Rao, S. M. Ahmad, and B. Uday Raj (1980), Geology and geochemistry of paragneisses from the Javanahalli schist belt, Karnataka, India, *J. Geol. Soc. India*, *21*, 577–592.

Narayana, B. L., S. M. Naqvi, P. Rama Rao, B. Uday Raj, and S. M. Ahmad (1983), Geology and geochemistry of Javanahalli schist belt, Karnataka, India, in *Precambrian of South India*, edited by S. M. Naqvi and J. J. W. Rodger, pp. 143–157, Geol. Soc. India, Bangalore, India.

Nitescu, B., A. R. Cruden, and R. C. Bailey (2006), Crustal structure and implications for the tectonic evolution of the Archean Western Superior craton from forward and inverse gravity modeling, *Tectonics*, *25*, TC1009, doi:10.1029/2004TC001717.

Passchier, C. W., S. W. J. Den Brok, J. Van Gool, M. Marker, and G. Manatschal (1997), A laterally constricted shear zone system—The Nordre Stromfjord steep belt, Nagssugtoqidian orogen, W. Greenland, *Terra Nova*, *9*, 199–202, doi:10.1111/j.1365-3121.1997.tb00012.x.

Peucat, J. J., B. Mahabaleswar, and M. Jayananda (1993), Age of younger tonalitic magmatism and granulitic metamorphism in the south Indian transition zone (Krishnagiri area): Comparison with older Peninsular gneisses from the Gorur-Hassan area, *J. Metamorph. Geol.*, *11*, 879–888, doi:10.1111/j.1525-1314.1993.tb00197.x.

Peucat, J. J., H. Bouhallier, C. M. Fanning, and M. Jayananda (1995), Age of the Holenarsipur greenstone belt, relationships with the surrounding gneisses (Karnataka, south India), *J. Geol.*, *103*, 701–710, doi:10.1086/629789.

Raase, P., M. Raith, D. Ackermand, and R. K. Lal (1986), Progressive metamorphism of mafic rocks from greenschist to granulite facies in the Dharwar Craton of south India, *J. Geol.*, *94*, 261–282, doi:10.1086/629027.

Ramsay, J. G. (1967), *Folding and Fracturing of Rocks*, McGraw-Hill, New York.

Rey, P. F., and G. Houseman (2006), Lithospheric scale gravitational flow: The impact of body forces on orogenic processes from Archaean to Phanerozoic, in *Analogue and Numerical Modelling of Crustal-Scale Processes*, edited by S. J. H. Buiter and G. Schreurs, *Geol. Soc. Spec. Publ.*, 253, 153–167, doi:10.1144/GSL.SP.2006.253.01.08.

Rogers, A. J., J. Kolb, F. M. Meyer, and R. A. Armstrong (2007), Tectono-magmatic evolution of the Hutti-Maski Greenstone Belt, India: Constrained using geochemical and geochronological data, *J. Asian Earth Sci.*, *31*(1), 55–70, doi:10.1016/j.jseaes.2007.04.003.

Ross, A. R., L. D. Brown, P. Pananont, K. D. Nelson, S. Klemperer, S. Haines, W. J. Zhao, and J. R. Guo (2004), Deep reflection surveying in central Tibet: Lower-crustal layering and crustal flow, *Geophys. J. Int.*, *156*(1), 115–128, doi:10.1111/j.1365-246X.2004.02119.x.

Royden, L. H., B. C. Burchfiel, and R. D. van der Hilst (2008), The geological evolution of the Tibetan Plateau, *Science*, *321*, 1054–1058, doi:10.1126/science.1155371.

Sanchez, V. I., M. A. Murphy, W. R. Dupre, L. Ding, and R. Zhang (2010), Structural evolution of the Neogene Gar Basin, western Tibet: Implications for releasing bend development and drainage patterns, *Geol. Soc. Am. Bull.*, *122*(5–6), 926–945, doi:10.1130/B26566.1.

Sandiford, M., and R. Powell (1991), Some remarks on high-temperature-low-pressure metamorphism in convergent orogens, *J. Metamorph. Geol.*, *9*, 333–340, doi:10.1111/j.1525-1314.1991.tb00527.x.

Saylor, J., P. DeCelles, G. Gehrels, M. Murphy, R. Zhang, and P. Kapp (2010), Basin formation in the High Himalaya by arc-parallel extension and tectonic damming: Zhada basin, southwestern Tibet, *Tectonics*, *29*, TC1004, doi:10.1029/2008TC002390.

Schulmann, K., O. Lexa, P. Stipska, M. Racek, L. Tajcmanova, J. Konopasek, J. B. Edel, A. Peschler, and J. Lehmann (2008), Vertical extrusion and horizontal channel flow of orogenic lower crust: Key exhumation mechanisms in large hot orogens?, *J. Metamorph. Geol.*, *26*, 273–297, doi:10.1111/j.1525-1314.2007.00755.x.

Seshadri, T. S., A. Chaudhuri, P. Harinadha Babu, and N. Chayapathi (1981), Chitradurga Belt, *Mem. Geol. Surv. India*, *112*, 163–198.

Sherrington, H. F., G. Zandt, and A. Frederiksen (2004), Crustal fabric in the Tibetan Plateau based on waveform inversions for seismic anisotropy parameters, *J. Geophys. Res.*, *109*, B02312, doi:10.1029/2002JB002345.

Tapponnier, P., Z. Q. Xu, F. Roger, B. Meyer, N. Arnaud, G. Wittlinger, and J. S. Yang (2001), Oblique stepwise rise and growth of the Tibet Plateau, *Science*, *294*, 1671–1677, doi:10.1126/science.105978.

Taylor, M., A. Yin, F. J. Ryerson, P. Kapp, and L. Ding (2003), Conjugate strike-slip faulting along the Bangong-Nujiang suture zone accommodates coeval east-west extension and north-south shortening in the interior of the Tibetan Plateau, *Tectonics*, *22*(4), 1044, doi:10.1029/2002TC001361.

Tikoff, B., C. Teyssier, and C. Waters (2002), Clutch tectonics and the partial attachment of lithospheric layers, *EGU Stephan Mueller Spec. Publ. Ser.*, *1*, 57–73, doi:10.5194/smsps-1-57-2002.

Van Der Velden, A. J., F. A. Cook, B. J. Drummond, and B. R. Goleby (2006), Reflections of the Neoarchean: A global perspective, in *Archean Geodynamics and Environments*, edited by K. Benn, J. C. Mareschal, and K. C. Condie, pp. 255–265, AGU, Washington, D. C.

Vanderhaeghe, O., and C. Teyssier (2001), Partial melting and flow of orogens, *Tectonophysics*, *342*, 451–472, doi:10.1016/S0040-1951(01)00175-5.

Vassallo, J. J., and C. J. L. Wilson (2002), Palaeoproterozoic regional-scale non coaxial deformation: An example from eastern Eyre Peninsula, South Australia, *J. Struct. Geol.*, *24*, 1–24, doi:10.1016/S0191-8141(01)00043-8.

Vasudev, V. N., B. Chadwick, A. P. Nutman, and G. V. Hedge (2000), Rapid development of the Late Archaean Hutti schist belt, Northern Karnataka: Implications of new field data and SHRIMP U-Pb zircon ages, *J. Geol. Soc. India*, *55*, 529–540.

Wells, P. R. A. (1980), Thermal models for the magmatic accretion and subsequent metamorphism of continental crust, *Earth Planet. Sci. Lett.*, *46*(2), 253–265, doi:10.1016/0012-821X(80)90011-4.

Yang, Y. Q., M. Liu, and S. Stein (2003), A 3-D geodynamic model of lateral crustal flow during Andean mountain building, *Geophys. Res. Lett.*, *30*(21), 2093, doi:10.1029/2003GL018308.

Zhang, P. Z., Z. Shen, M. Wang, W. J. Gan, R. Burgmann, and P. Molnar (2004), Continuous deformation of the Tibetan Plateau from global positioning system data, *Geology*, *32*, 809–812, doi:10.1130/G20554.1.